Article

Estimation of Electron Distribution over Dinuclear Organometallic Molecular Wires by "IR Tag" Analysis of Ancillary Acyl-Cp Ligands

Yuya Tanaka,* Hiroki Takahashi, and Munetaka Akita*

Cite This: ACS Org. Inorg. Au 2022, 2, 327−342

Read Online

ACCESS | Metrics & More | Article Recommendations | Supporting Information

ABSTRACT: Understanding the details of electronic properties of mixed-valence (MV) states of organometallic molecular wires is essential to gain insights into electron transfer phenomena. Although the field of MV chemistry is matured, there remain issues to be solved, which cannot be accessed by the conventional analytical methods. Here, we describe the synthesis and properties of diruthenium bridging (diethynylbenzene)diyl wires, (μ-p and m-$C{\equiv}C{-}C_6H_4{-}C{\equiv}C$){RuCp^R(dppe)}$_2$ **1**, with the acyl-substituted cyclopentadienyl rings [Cp^R: Cp^e; η^5-C_5H_4COOMe (**a**-series: ester

derivatives), Cp^a; η^5-C_5H_4COMe (**b**-series: acetyl derivatives)], which are installed as IR-tags to estimate electron densities at the metal centers in the MV species. The electrochemical and IR/near IR-spectroelectrochemical studies reveal that the two metal centers in the $para$-isomers p-**1a,b$^+$** interact with each other more strongly than those in the $meta$-isomers m-**1a,b$^+$**. Electron-spin resonance study also supports the radicals being delocalized over the Ru-(p-$C{\equiv}C{-}C_6H_4{-}C{\equiv}C$)−Ru moieties in p-**1a,b$^+$**. The spectroelectrochemical IR study shows significant higher-energy shifts of the $\nu(C{=}O)$ vibrations brought about upon 1e-oxidation. Spectral simulation on the basis of the Bloch equations allows us to determine the electron transfer rate constants (k_{et}) between the two metal centers being in the orders of 10^{12} s^{-1} (p-**1$^+$**) and 10^9 s^{-1} (m-**1$^+$**). The shifts of the $\nu(C{=}O)$ bands reveal that the charge densities on the $para$-isomers p-**1a,b$^+$** are widely delocalized over the Ru-(p-$C{\equiv}C{-}C_6H_4{-}C{\equiv}C$)−Ru linkages in contrast to the $meta$-isomers m-**1a,b$^+$**, where the electron densities are mainly localized on the metal fragments, as supported by the density functional theory and time-dependent density functional theory studies as well as comparison with the reference mononuclear acetylide complexes, $C_6H_5{-}C{\equiv}C{-}RuCp^R$(dppe) **2**. We have successfully demonstrated that the carbonyl groups (>C=O) in the ancillary Cp ligands also work as IR-tags to report detailed information on the electron densities at the metal centers and the electron distribution over MV complexes as well.
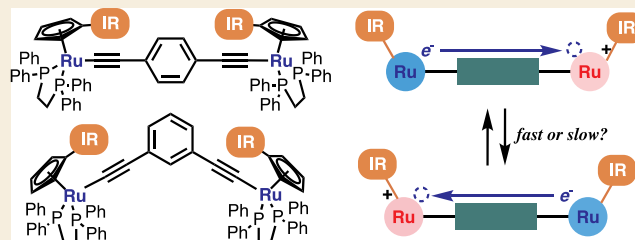
KEYWORDS: mixed-valence species, ruthenium complex, infra-red tag, metal alkynyl complex, acylcyclopentadienyl ligand

■ INTRODUCTION

Mixed-valence (MV) chemistry of inorganic and organometallic complexes has been continuously developed to deepen the fundamental understanding of the electron transfer processes involved since the discovery of the monumental Creutz−Taube ion, [Ru(NH$_3$)$_5$-μ-pyrazine-Ru(NH$_3$)$_5$]$^{5+}$, in 1969, and the complex is regarded as the first MV coordination complex.[1] A central issue of this area is the understanding of the electronic properties of the MV state, that is, the extent of charge delocalization over the molecule and the electron transfer rate between the two redox sites. Robin and Day classified the MV complexes into three categories, that is, a fully delocalized state (class III), a fully localized state (class I), and an intermediate state between them (class II).[2] For the determination of the class, various physicochemical methods such as electrochemistry, electron-spin resonance (ESR), Mössbauer, X-ray photoelectron spectroscopy (XPS), and UV−vis−NIR (near IR) absorption spectroscopy have been used. However, discussion of the classification is not always straightforward. For example, the comproportionation constant

(K_C), which indicates the thermodynamic stability of the MV species, can be readily obtained from the CV study, but the redox potentials are strongly influenced by the environment such as the counter anions and the solvents used for the measurements.[3,4] The intervalence charge transfer (IVCT) band in the NIR region observed for the MV species is commonly used for their classification. According to the Marcus−Hush theorem,[5] the strength of electronic coupling (V_{ab}) can be determined from the IVCT band parameters. Because, however, inorganic and organometallic MV complexes frequently show multiple and overlapped NIR bands, identification of the IVCT band is frequently ambiguous.[6]
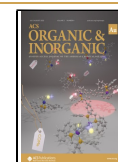
Scheme 1. Schematic Descriptions of Metal-Localized and Bridge-Localized States for CP(dppe)Ru−C≡C−Ar−C≡C−Ru(dppe)CP Complexes Associated with Their Conformational Isomers
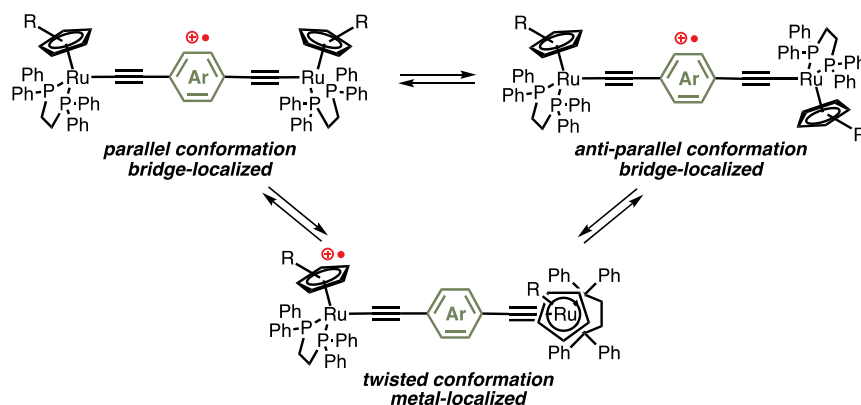
IR spectroscopy is another powerful method to evaluate the electronic structure of MV complexes because the timescale of IR spectroscopy is short enough ($\sim 10^{-12}$ s) to evaluate electron transfer processes of MV complexes. In the seminal work by Kubiak and Ito using the IR tag technique, they reported the electron transfer rates for a series of MV complexes composed of the two μ_3-oxotriruthenium clusters bridged by a pyrazine linker on the basis of the detailed analysis of the IR data of the terminal CO ligands.[7] The successful IR analysis involving line shape analysis afforded the electron transfer rate constants (k_{et}) of the MV complexes, which were in the order of 10^{12} s^{-1}. On the other hand, studies on organometallic MV systems by the IR-tag technique are rare. Winter reported dinuclear MV complexes with the vinylruthenium fragments having supporting CO ligands,[8,9] and on the basis of the spectroelectrochemical IR study, the localized and delocalized charge states were successfully distinguished. While the methods are relatively simple and provide a variety of information, the studies reported to date are mainly limited to the MV complexes with CO ligands showing intense IR absorptions.[10−13]

Multinuclear complexes bearing the group 8 metal acetylide fragments, CP(dppe)M−C≡C [M = Fe, Ru; CP = cyclopentadinyl (Cp) or 1,2,3,4,5-pentamethylcyclopentadienyl (Cp*); dppe = 1,2-bis(diphenylphosphino)ethane], have been extensively studied due to the thermodynamic stability of their 1e-oxidized monocationic MV states caused by the electron-rich metal fragments, and such a feature allows studies of a wide variety of one- and two-dimensional multinuclear species.[14−19] Deep understanding of electronic structures of MV is important. For example, Low proposed another MV state called "bridge-localized state". 1e-Oxidation of Cp*-(dppe)Ru−C≡C−Ar−C≡C−Ru(dppe)Cp* (Ar = 1,4-benzenediyl, 1,4-naphthalenediyl, and 9,10-anthracenediyl) formed the MV species, where the positive charge is mainly localized on the organic bridging part rather than on the metal centers, and the trend became remarkable as the π-system of the bridging aromatic ring was enlarged.[20] Furthermore, details of the electronic structures of such "bridge-localized" states have been investigated on the basis of a theoretical study, which showed that the conformation of the Ru fragments is a dominant factor for the charge localization/delocalization. Detailed density functional theory (DFT) analyses by Kaupp suggested that the parallel and antiparallel conformational isomers with respect to the two Cp*Ru(dppe) fragments

exhibit the bridge-localized state, while the twisted conformation causes the metal-localized state (Scheme 1).[21]

To *experimentally* clarify the charge distribution, the electron density, that is, the oxidation states, at the ruthenium centers should be determined. We envisaged that new metal fragments with IR-active pendants should provide information on the electron density at the metal centers. Herein, we report the synthesis and characterization of dinuclear ruthenium complexes bridged by the p- and m-(diethynylbenzene)diyl ligands (**1**) with the Cp ligands having the IR-active acyl groups, Cp^{R}Ru(dppe) [Cp^R: Cp^e; η^5-C$_5$H$_4$COOMe (a-series: ester derivatives), Cp^a; η^5-C$_5$H$_4$COMe (b-series: acetyl derivatives)], together with the reference mononuclear complexes **2**. The electronic structures of the MV species thereof are analyzed on the basis of the ν(C=O) vibrations (Figure 1). Dinuclear MV complexes with (diethynylbenzene)diyl bridges have been studied extensively[22,23] and thus would be suitable motifs to verify the usefulness of IR-tags.
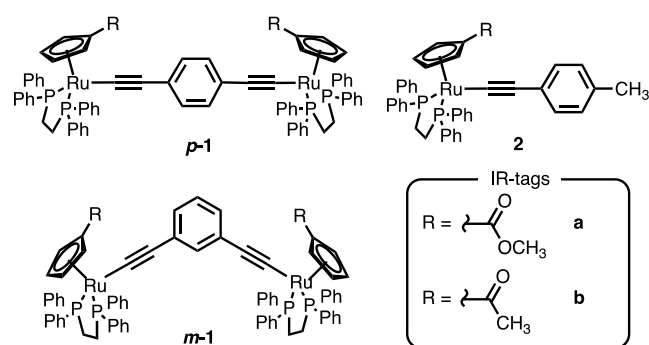
Figure 1. Structures of mono- and di-nuclear complexes with IR-active ruthenium fragments studied in the present work.

RESULTS AND DISCUSSION

Synthesis and Characterization

Ruthenium chloride precursors, Cp^{R}Ru(dppe)Cl [R = COOCH$_3$ (**3a**), COCH$_3$ (**3b**)], were synthesized by the reaction of the Cp^{R}Na derivatives with RuCl$_2$(PPh$_3$)$_3$, followed by the ligand substitution with dppe in good yields in a manner similar to the synthesis of the Cp derivative.[24] Sequential treatment of **3a** and **3b** with AgBF$_4$ and the appropriate terminal alkyne in the presence of DBU afforded the corresponding mono- and di-nuclear complexes **1** and **2** in

45−75% yields (Scheme 2). It is noted that the conventional synthetic method using Na^+/K^+ PF_6^{-25} instead of the silver salt

Scheme 2. Synthetic Routes to 1 and 2
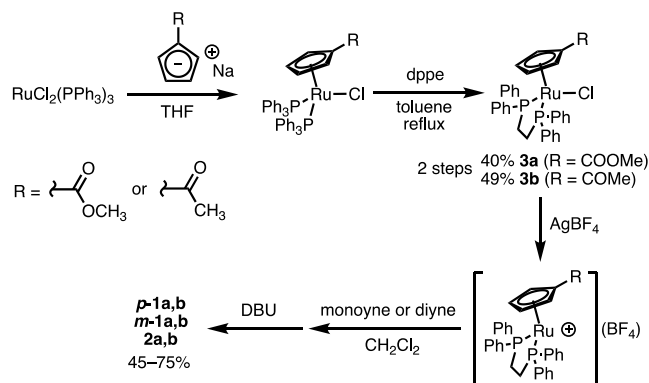
left the starting chloride precursors **3** untouched probably due to the stronger Ru−Cl bonds caused by the electron-withdrawing acyl groups.

Spectroscopic data of the complexes are summarized in Table 1. ^{1}H NMR spectra of the mononuclear complexes **2a**

Table 1. Selected Spectroscopic Data for 1−3

| | ^{1}H NMR/δ_H[a] | | | IR/cm^{-1e} | |
complex	C_5H_4-R[b]	CH_3 in R[c]	^{31}P NMR/δ_P[a],[d]	$\nu(C\equiv C)$	$\nu(C=O)$
p-1a (R = COOMe)	5.44, 4.57	3.43	84.9	2081	1703
p-1b (R = COMe)	5.51, 4.52	1.90	83.9	2081	1650
m-1a (R = COOMe)	5.48, 4.58	3.41	84.9	2075	1703
m-1b (R = COMe)	5.53, 4.53	1.92	84.1	2074	1650
2a (R = COOMe)	5.47, 4.60	3.47	85.0	2085	1703
2b (R = COMe)	5.54, 4.54	1.95	83.9	2085	1650
3a (R = COOMe)	5.24, 4.14	3.60	79.1		1705[f]
3b (R = COMe)	5.30, 4.14	1.95	78.2		1653[f]

[a]In $CDCl_3$. [b]Multiplet signals, 4H for each signal of **1** and 2H for each signal of **2** and **3** [c]Singlet signals (3H). [d][1]H-decoupled spectra, singlet signals. [e]In CH_2Cl_2. [f]As KBr pellets.

and **2b** contain the methyl signals for the ester and acetyl groups at 3.60 and 1.95 ppm, respectively. ^{31}P{^{1}H} NMR signals for the dppe ligands are observed at 85.0 (**2a**) and 83.9 (**2b**) ppm, which are comparable to those for the acetylides bearing the CpRu(dppe) ($\delta_p \sim 87$ ppm) and Cp*Ru(dppe) ($\delta_p \sim 81$ ppm) groups.[22] Symmetric structures of the dinuclear complexes **1** in solution are confirmed by the single sets of the ^{1}H and ^{31}P NMR signals for the Cp^R (R = $COOCH_3$, $COCH_3$) and dppe ligands. The $\nu(C\equiv C)$ and $\nu(C=O)$ vibrations are observed as single bands around 2080 and 1650−1705 cm^{-1}, respectively. In general, diethynylbenzene compounds show single $\nu(C\equiv C)$ vibrations due to the asymmetric coupling of the two $C\equiv C$ vibrations, while those of the symmetric modes are usually silent.[26] The $\nu(C\equiv C)$ vibrational stretching frequencies for the ester and acetyl

derivatives **1−2** are virtually identical, suggesting that the electron densities at the Ru centers are similar. Molecular structures of **1−2** determined by X-ray crystallography are shown in Figure 2. The Ru atoms in **1** and **2** adopt the three-legged piano stool geometries and the Ru−C≡ distances ranging between 2.003 and 2.020 Å are comparable to that for CpRu(dppe)−C≡C−C_6H_5 (**4**; Ru−C: 2.001 Å, Ru−P: 2.238 Å, Ru−C_{cp}: 2.257 Å).[27,28] However, the slightly longer Ru−P bonds ($\Delta d = 0.009−0.019$ Å) and the shorter Ru−C_{cp} bonds (Δd 0.005−0.018 Å) compared to those in **4** should be due to the decreased and increased back donation from the ruthenium centers, respectively. The $Cp_{centroid}$−Ru−Ru−$Cp_{centroid}$ dihedral angles are 180° (**p-1a/b**), 117° (**m-1a**), and 125° (**m-1a**). The through-space Ru−Ru distances are determined for the *para*- and *meta*-isomers to be ~12.1 and ~10.7 Å, respectively.

Electrochemical Study

Redox properties of the Ru complexes were examined by cyclic voltammetry (Figure 3 and Table 2). CV charts of the mononuclear complexes **2** contain single partially reversible redox waves with half-wave potential of around 40 mV (vs Cp_2Fe/Cp_2Fe^+ couple), which are anodically shifted by 120 mV compared to that of Cp(dppe)Ru−C≡C−C_6H_5 **4**, as a result of the decreased electron densities at the metal centers caused by the electron-withdrawing acyl substituents on the Cp rings. The $E_{1/2}$ values of **2a,b** are almost identical, suggesting the comparable electron-withdrawing effects of the ester and acetyl groups. For the dinuclear *para*-isomers **p-1a,b**, two fully reversible waves around −190 and 70 mV (vs $FeCp_2/FeCp_2^+$ couple, 100 mV/s) are observed. The first oxidation processes are shifted cathodically compared to the mono-nuclear complexes **2** due to the electronic interactions between the two ruthenium centers and also inductive effects due to the attachment of the two electron-rich CpRu(dppe) donors to the bridging ligand. From the separation of the two redox waves (ΔE), the comproportionation constants (K_C) are determined to be 1.35×10^4 (**p-1a**) and 9.00×10^3 (**p-1b**). In contrast to the *para*-isomers **p-1**, the *meta*-isomers **m-1** show two irreversible redox waves in the range of 0−400 mV when scanned at 100 mV/s.

Upon increasing the scan rate to 1000 mV/s, reversibility of the waves was improved. When the range of −500 to 200 mV was swept at a rate of 100 mV/s, partially reversible 1e-oxidation processes were observed, indicating that the monocationic species of the *meta*-isomers **m-1a,b** are stable on the timescale of the electrochemical measurements. Then, differential pulse voltammetry (DPV) measurements (see the Supporting Information) was carried out to obtain the K_C values of 6.9×10^2 (**m-1a**) and 8.4×10^2 (**m-1b**), which are considerably smaller than those of the *para*-isomers **p-1a,b** due to the connection through the cross-conjugated meta-linkages. In spite of the small K_C values for the *meta*-isomers, the monocationic species turned out to be populated enough in solutions.

The redox potentials and K_C values of the ester and acetyl derivatives **p-1** ($K_C \sim 1 \times 10^4$) and **m-1** ($K_C \sim 7−8 \times 10^2$) are very similar, suggesting that the electronic interactions between the metal centers are akin to each other. The K_C values of the dinuclear *para*-isomers **p-1** are comparable to that of the related Cp analogue [**p-5**, (μ-*p*-C≡C−C_6H_4−C≡C)-{$RuCp^R$(dppe)}$_2$]. Similarly, the K_C values of the *meta*-isomers **m-1** are very close to that of the Cp* derivative **6** [μ-*m*-C≡C−C_6H_4−C≡C){$RuCp^*$(dppe)}$_2$].[28,29] These facts suggest
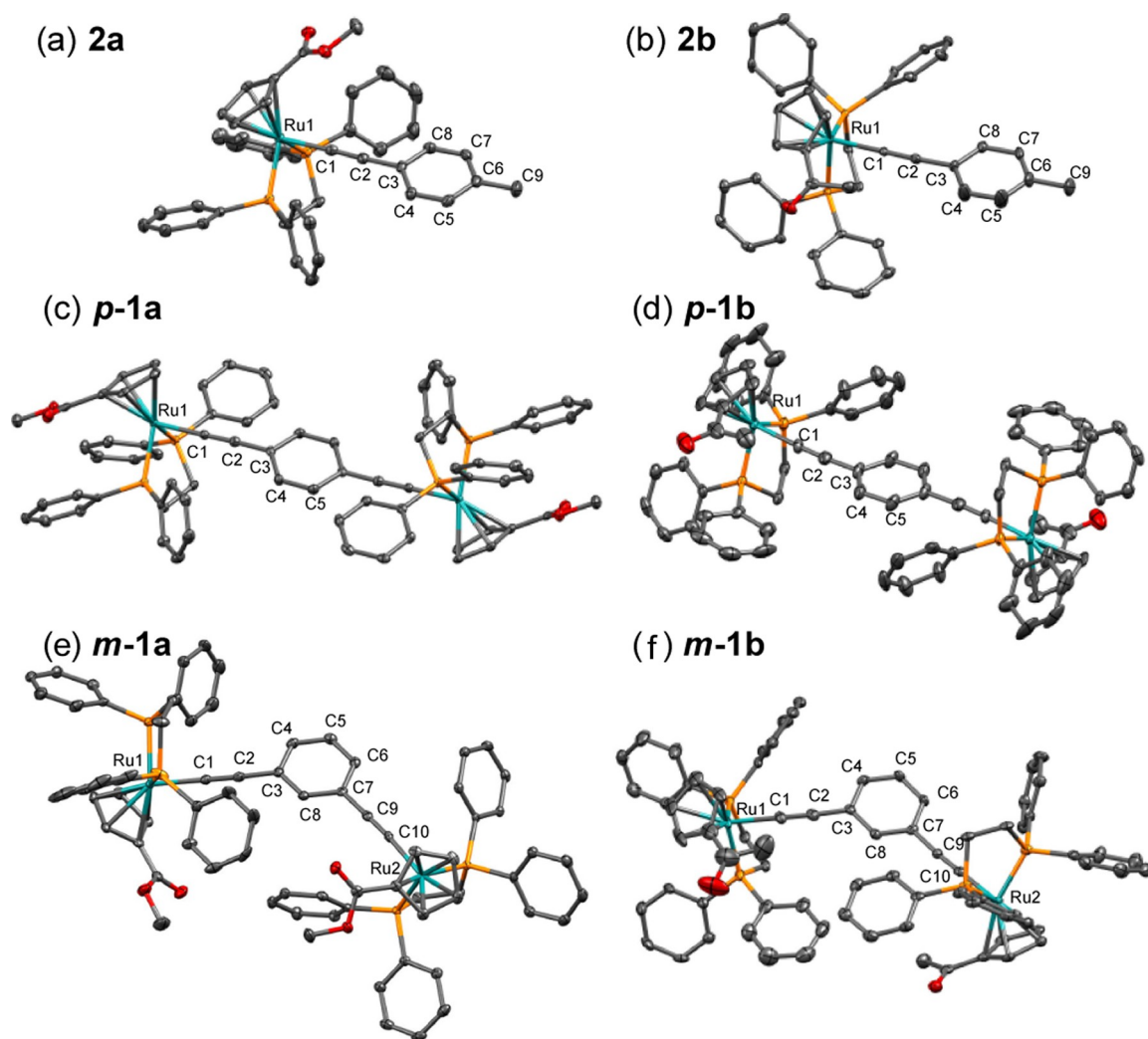
Figure 2. ORTEP diagrams of mono- (2) and di-nuclear complexes (1) drawn with the thermal ellipsoids at 50% level. Hydrogen atoms and solvents are omitted for clarity.

that the thermodynamic stability of the MV species of the dinuclear complexes is rather insensitive to the electron-donating properties of the substituted Cp rings.

Spectroelectrochemical IR Study

Spectroelectrochemical IR studies were performed for CH_2Cl_2 solutions in the presence of 0.1 M $[NBu_4][PF_6]$ as an electrolyte by using an OTTLE cell (Figures 4 and 5 and Table 3). We first examined the mononuclear reference complexes **2a,b**, which showed single C=O stretching vibrations around 1700 cm^{-1} (for the ester groups) and around 1650 cm^{-1} (for the acetyl groups) (Figure 4a,b). In addition, the intense bands observed around 2100 cm^{-1} were unequivocally assigned to the C≡C stretching vibrations. Upon oxidation of **2**, the C≡C and C=O bands were replaced by the bands at around 1930 cm^{-1} [ν(C≡C)] and 1728 (for **2a**) and 1686 cm^{-1} (for **2b**) [ν(C=O)] with the decreased intensities. It is noted that isosbestic points were observed, indicating the occurrence of a two-component system involving direct conversions from **2** to **2$^+$**. In addition to the significant shifts of the C≡C stretching bands to lower energies ($\Delta\nu \sim$ 150 cm^{-1}), the C=O bands also shifted to higher energies by 25 cm^{-1} for **2a** (1728 cm^{-1}) and 36 cm^{-1} for **2b** (1686 cm^{-1}) (Figure 5a,b), suggesting that

the carbonyl substituents are sensitive to the electron densities at the ruthenium centers.

Encouraged by these results, the spectroelectrochemical IR measurements were extended to the dinuclear complexes (**1**). For the *para*-isomers *p*-**1a,b** (Figures 4c and 5c,d), two-step oxidation processes were observed. Upon application of bias voltages, the weak ν(C≡C) vibrations of the neutral species *p*-**1a,b** were replaced by the intense bands around 1970−2020 cm^{-1} and the weak bands around 2070 and 1920 cm^{-1}, which were assignable to *p*-**1a,b$^+$**. The four ν(C≡C) vibrations observed for *p*-**1a,b$^+$** are similar to those reported for the Cp* analogues and are derived from the occurrence of rotamers (Figure 1).[30] Further oxidation caused the second process resulting in the replacement of the bands around 2000 cm^{-1} by the new weak bands around 1940 cm^{-1}, which were ascribed to the dioxidized species *p*-**1a,b^{2+}**. For the first step, similar observations were reported for the monocationic dinuclear ruthenium complexes with the Cp* and Cp rings.[20,28] The large changes of the intensities may be caused by the coupling of two C≡C bonds. Along with the changes of the ν(C≡C) bands, the C=O vibrations were also shifted in a stepwise manner (Figure 5c). For *p*-**1a**, the ν(C=O) bands appeared at 1703 (*p*-**1a**), 1712 (*p*-**1a$^+$**), and 1727 cm^{-1} (*p*-**1^{2+}**). Similarly, for *p*-**1b**, the sequential and stepwise shifts of the ν(C=O)
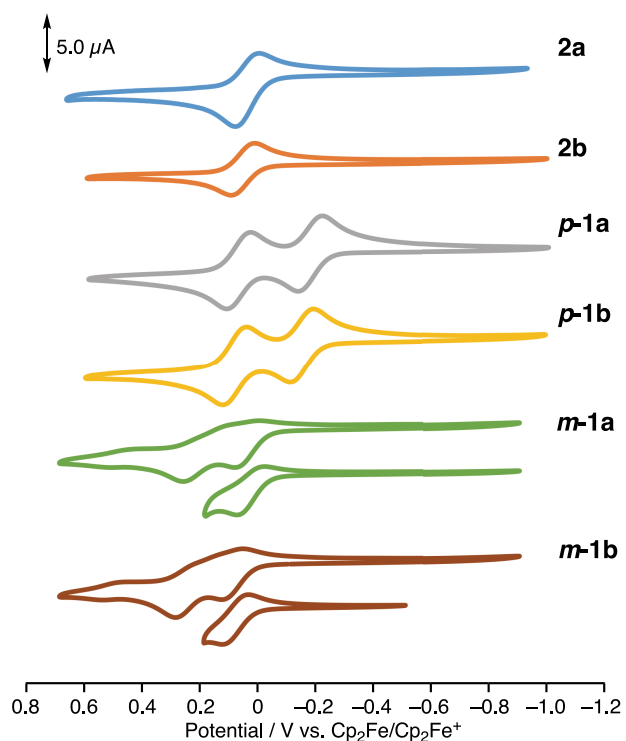
Figure 3. Cyclic voltammograms of 1−2 ([complex] = ∼1.0 mM in CH$_2$Cl$_2$, [NBu$_4$][PF$_6$] = 0.1 M, W.E. and C.E. Pt, R.E. Ag/Ag$^+$, scanned at 100 mV/s).

band of the acetyl groups was observed: 1651 cm^{-1} (**p-1b**) → 1667 cm^{-1} (**p-1b$^+$**) → 1685 cm^{-1} (**p-1b^{2+}**) (Figure 5d). It is noted that the ν(C=O) vibration energies of the neutral and dicationic species for **p-1a,b** are very similar to those of the neutral and monocationic species of the mononuclear complexes **2a,b**, suggesting that the electron densities at the ruthenium centers in the neutral and cationic species are similar with each other. Interestingly, during the oxidation processes, the intensities of the ν(C≡C) bands drastically changed, while those of the ν(C=O) bands were not affected significantly. This is because the ν(C≡C) vibration is symmetry forbidden, and the degree of charge localization/delocalization strongly affects the symmetry of the molecules, leading to the drastic changes of the intensity. In addition, vibrations of the C≡C bonds in a molecule (such as **2**) may couple to show, for example, symmetrically and antisymmetrically coupled vibrations and make analysis difficult. Thus, analysis based on the ν(C=O) bands provides another merit.

Spectroelectrochemical IR measurements of the *meta*-isomers **m-1** were also performed (Figures 4e,f and 5e,f), and the following changes were noted for ν(C≡C) [∼2075 cm^{-1} (**m-1**) → ∼2000 cm^{-1} (very weak: **m-1$^+$**) → ∼1931, 2000, 2070 cm^{-1} (**m-1^{2+}**)] and for ν(C=O) [1703 cm^{-1} (**m-1a**) → 1726, 1704 cm^{-1} (**m-1a$^+$**) → 1728 cm^{-1} (**m-1a^{2+}**); 1650 cm^{-1} (**m-1b**) → 1651, 1686 cm^{-1} (**m-1b$^+$**) → 1686 cm^{-1} (**m-1b^{2+}**)]. The ν(C=O) bands of **m-1a$^+$** were overlapped with those of **m-1a** and **m-1a^{2+}**.

To obtain electron transfer rate constants (k_{et}) of the MV species, simulation with the VIBEX GL program, which is based on the Bloch equation, was performed (Figures 6 and 7).[7,31] As shown in Figure 7, upon changing the k_{et} values in the range between 10^{11} and 10^{13} s^{-1}, the shapes of the simulated spectra apparently changed, and the k_{et} values were obtained by the fitting analysis of the experimental and calculated spectra. The band shapes are successfully reproduced for **p-1a$^+$**, **p-1b$^+$**, and **m-1a$^+$**, although the shoulder band at 1728 cm^{-1} should be taken into account for **p-1a$^+$**.[32] Overlapping with the stretching bands of the Ph groups hindered the line fitting analysis of **m-1b$^+$**.

The k_{et} values of **p-1a$^+$** and **p-1b$^+$** are determined to be 6 × 10^{12} and 6 × 10^{12} s^{-1}, respectively. The k_{et} value for **m-1a$^+$** was estimated to be at most 1 × 10^{10} s^{-1} because in the k_{et} region below 1 × 10^{10} s^{-1}, the spectral change is rather insensitive to k_{et}, and therefore, k_{et} cannot be determined accurately on the basis of the line shape analysis.

Spectroelectrochemical UV−Vis−NIR Study

To determine electronic coupling V_{ab} on the basis of the NIR spectra of **1$^+$**, spectroelectrochemical measurements in an OTTLE cell were performed for CH$_2$Cl$_2$ solutions of **1** containing 0.1 M [NBu$_4$][PF$_6$] as an electrolyte (Figure 8 and Table 4). For the neutral species **1**, UV absorption bands were observed around 290−360 nm, which were characteristic π−π* bands admixed with ligand-to-metal charge transfer bands.[20] Upon application of the bias voltage to the *para*-isomers **p-1a,b**, the UV bands disappeared and new bands assignable to the monocationic species **p-1a,b$^+$** appeared in the visible (500 nm, π−π*) and NIR regions (1000−2000 nm) (for the assignments, see below). Upon increment of the bias voltage, the bands due to **p-1a,b$^+$** were replaced by the new bands around 750 nm, which were ascribed to the dicationic species **p-1a,b^{2+}**. On the other hand, the absorption band for the neutral *meta*-species **m-1a** at 298 nm was weakened upon 1e-oxidation and the new bands for **m-1a$^+$** appeared at 796 and 1326 nm. Further oxidation led to the replacement of the NIR band by that at 1460 nm (for **m-1a^{2+}**) together with the increase of the intensity of the band at 796 nm, suggesting

Table 2. Selected Electrochemical Data for 1−2 and Related Complexes[a]

compound	$E^1_{1/2}$/mV [i_{pc}/i_{pa}]	$E^2_{1/2}$/mV [i_{pc}/i_{pa}]	ΔE/mV	K_C
p-1a	−190 (−195) [1.0]	55 (50) [1.0]	245 (245)	1.35 × 10^4
p-1b	−160 (−165) [1.0]	70 (65) [1.0]	230 (230)	9.0 × 10^3
m-1a	21 (5) [0.4]	(170) [0.4]	(165)	6.9 × 10^2
m-1b	75 (55) [0.5]	238 (225) [0.3]	163 (170)	8.4 × 10^2
2a	42 (25) [0.6]			
2b	45 (41) [0.9]			
RuC≡CC$_6$H$_5$ (4)[15]	−80			
(μ-C≡C−p-C$_6$H$_4$−C≡C) Ru$_2$ (5)[15]	−320	−90	230	9.0 × 10^3
(μ-C≡C−m-C$_6$H$_4$−C≡C) Ru$_2$* (6)[23]	−360	−200	160	6.7 × 10^2

[a]Data obtained by DPV measurements are shown in parentheses. **Ru** = Ru(dppe)Cp, **Ru*** = Ru(dppe)Cp*. Potentials vs Cp$_2$Fe/Cp$_2$Fe$^+$ couple.
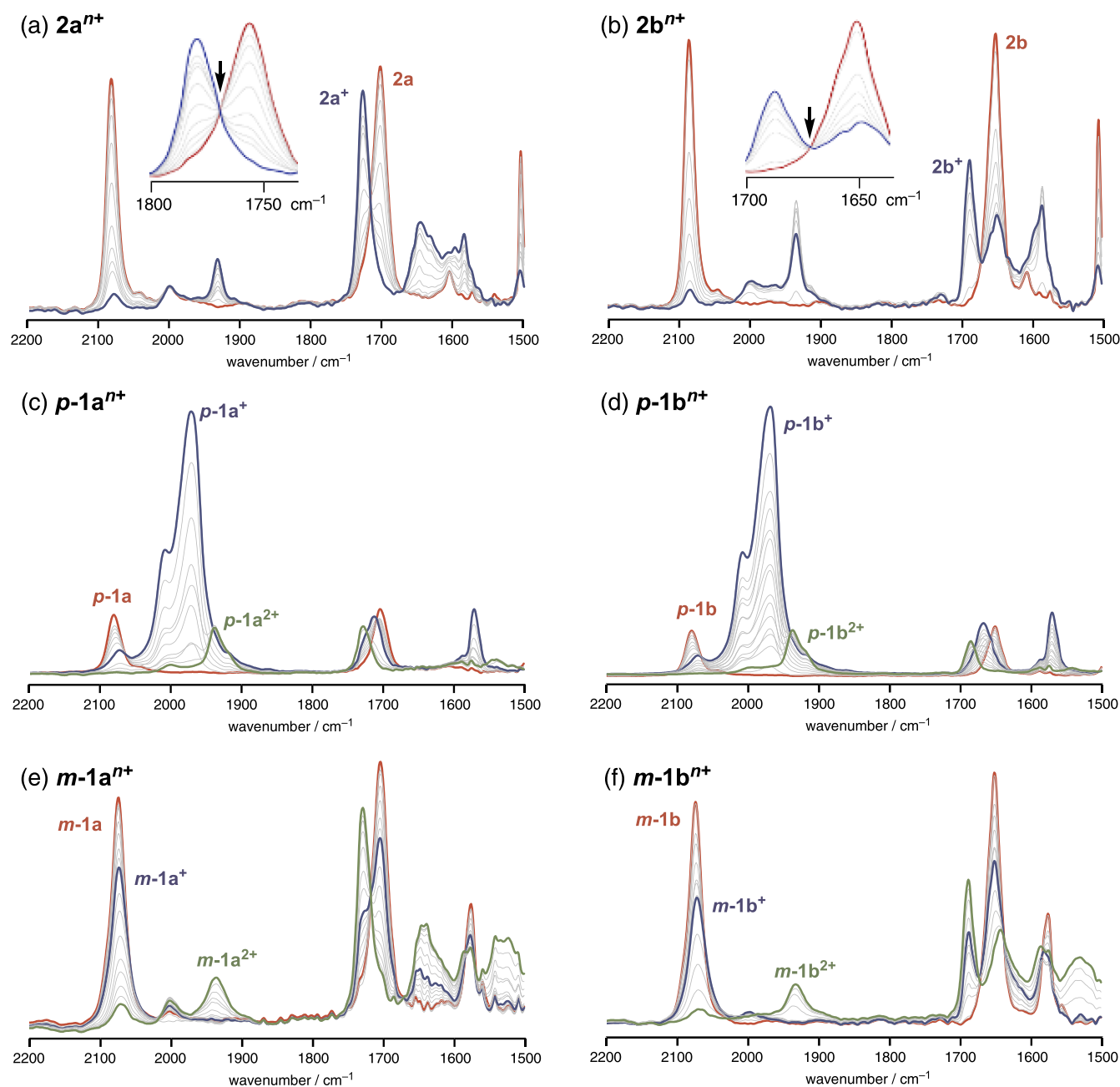
Figure 4. IR spectral changes of **1** and **2** observed in an OTTLE cell upon application of bias voltages ([complex] ∼ 10 mM, 0.1 M [NBu$_4$][PF$_6$] in CH$_2$Cl$_2$, W.E. and C.E. Pt, and R.E. Ag/Ag$^+$). The spectra for the three oxidation states are drawn in red (neutral), blue (monocation), and green (dication). The isosbestic points are indicated with the arrows in the insets.

sequential generation of the mono- and di-cationic species in accord with the IR measurements discussed above. For **m-1b**, we could not obtain reproducible results probably due to the instability of its cationic species, and thus, in the following section, discussion for the *meta*-isomers will be focused on **m-1a**.[33]

IVCT bands of organometallic MV complexes in the NIR region are frequently observed as overlapped multiple bands.[30] Therefore, the deconvolution analysis of the bands is essential to obtain V_{ab} values (Figure 9). For **p-1a$^+$**, the NIR bands were deconvoluted into the three Gaussian curves (bands A−C) as summarized in Table 5. For **p-1b$^+$**, essentially the same result as **p-1a$^+$** was obtained. Similarly, the IVCT bands of **m-1a$^+$** were deconvoluted into the two bands (bands A and B) in a

manner similar to the Cp* analogue **6$^+$**.[28,29] The bands for the *para*-isomers **p-1$^+$** ($\varepsilon \sim$ 17,000−20,000 M^{-1} cm^{-1}) were more intense than those for the *meta*-isomer **m-1a$^+$** ($\varepsilon \sim$ 1000−5000 M^{-1} cm^{-1}). For *para*-isomers **p-1$^+$**, the band widths calculated according to the Hush's theory [$\nu_{calc} = (2310 \times \nu_{max})^{1/2}$] were much larger than those of the bands A−C (Table 5), indicating stronger metal−metal interaction. The insensitivity of the NIR bands for *para*-isomers **p-1a,b$^+$** to the solvent polarity (acetone/CH$_2$Cl$_2$ = 98:2 vs CH$_2$Cl$_2$) (Figure 10) suggests the assignment of **p-1$^+$** as a class II/III border or class III species.[34] On the other hand, the value for the *meta*-isomer **m-1a$^+$** was comparable to the theoretical value, suggesting that **m-1a$^+$** is a class II species.
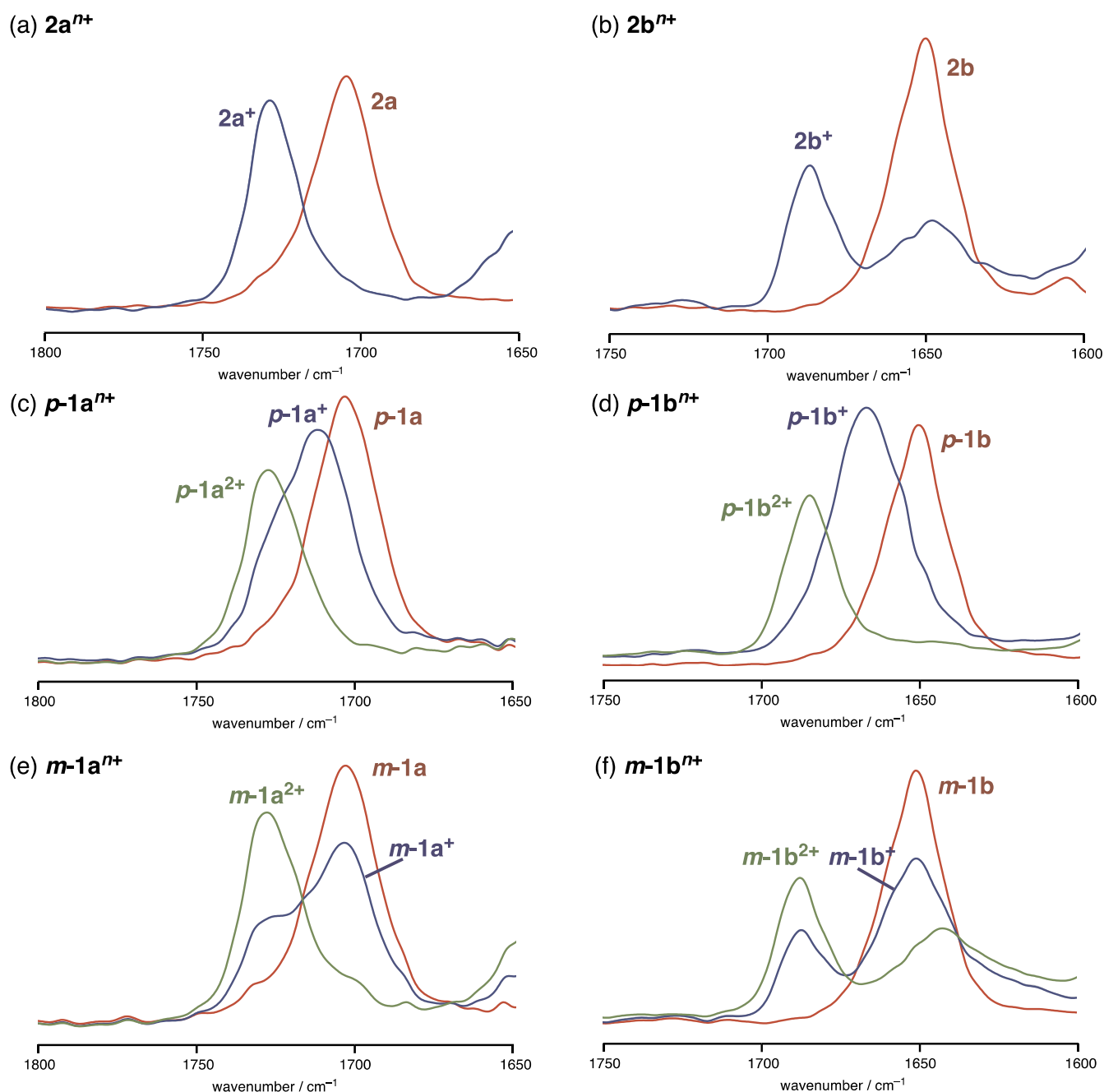
Figure 5. Parts of IR spectra [$\nu(C\equiv O)$ region] for $\mathbf{1}^{n+}$ and $\mathbf{2}^{n+}$ ($n = 0-2$) ([complex] = ~10 mM, [NBu$_4$][PF$_6$] = 0.1 M in CH$_2$Cl$_2$, W.E. and C.E. Pt, and R.E. Ag/Ag$^+$). The spectra for the three oxidation states are drawn in red (neutral), blue (monocation), and green (dication).

DFT and TD−DFT Calculations

In order to clarify the electronic structures of the MV species and to assign the NIR bands (Figures 11−13), DFT and TD-DFT calculations on $\mathbf{1}^{n+}$ and their Cp derivatives, $\boldsymbol{p}$-$\mathbf{5}^{n+}$ and $\boldsymbol{m}$-$\mathbf{5}^{n+}$ ([{(μ-p/m-C$\equiv$C−C$_6$H$_4$−C$\equiv$C){RuCp(dppe)}$_2$]$^{n+}$) (n = 0, 1), were performed. The structural optimization of $\mathbf{1}$ was started with the antiparallel conformations observed by the X-ray structural analysis. The Kohn−Sham orbitals of the neutral species are summarized in Figure 11. Bond lengths and angles well coincide with those obtained by the X-ray analysis. The highest occupied molecular orbitals (HOMOs) of the *para*-isomers $\boldsymbol{p}$-$\mathbf{1a,b}$ are delocalized over the Ru−C$\equiv$C−C$_6$H$_4$−C$\equiv$C−Ru frameworks, whereas the lowest unoccupied molecular orbitals (LUMOs) are localized on the dppe ligands.

These results are in accord with the results for the related dinuclear bridging acetylide complexes reported previously.[20] Similar features are noted for the *meta*-isomers $\boldsymbol{m}$-$\mathbf{1a,b}$. The HOMOs for the *para*-isomers $\boldsymbol{p}$-$\mathbf{1}$ are higher in energy by about 0.3 eV compared to those of the *meta*-isomers $\boldsymbol{m}$-$\mathbf{1}$, and the result is consistent with the trend of their redox potentials. On the other hand, the energy levels of the LUMOs are less sensitive to the connectivity of the central ring because the dppe ligands mainly constitute them. The HOMO and LUMO features for $\boldsymbol{p/m}$-$\mathbf{1a}$ are very similar to those for $\boldsymbol{p/m}$-$\mathbf{5}$. The HOMO and LUMO levels of $\boldsymbol{p/m}$-$\mathbf{5}$ are higher by about 0.2 and 0.4 eV, respectively, than those of the acyl derivatives $\mathbf{1}$, and the differences should derive from the electron-withdrawing acyl substituents.

Table 3. IR Data for $1^{n+}-2^{n+}$ ($n = 0-2$) Obtained with an OTTLE Cell^a

compound	n	$\nu(C{\equiv}C)$/cm^{-1}	$\nu(C{=}O)$/cm^{-1}
$2a^{n+}$	0	2085 (s)	1703 (s)
	1	2081 (w), 1934 (w)	1728 (s)
$2b^{n+}$	0	2085 (s)	1650 (s)
	1	2083 (w), 1932 (w)	1686 (s)
$p\text{-}1a^{n+}$	0	2081 (s)	1703 (s)
	1	2073 (w), 2009 (s), 1972 (s), 1920 (w)	1712 (s)
	2	2001 (w), 1938 (w)	1727 (m)
$p\text{-}1b^{n+}$	0	2081 (s)	1651 (s)
	1	2072 (w), 2009 (s), 1969 (s), 1919 (w)	1667 (s)
	2	1995 (w), 1938 (w)	1685 (m)
$m\text{-}1a^{n+}$	0	2075 (s)	1703 (s)
	1	2073 (s), 2001 (w)	1704 (m), 1726 (m)
	2	2072 (w), 1934 (w)	1728 (m)
$m\text{-}1b^{n+}$	0	2074 (s)	1650 (s)
	1	2071 (w), 2001 (w)	1651 (m), 1686 (m)
	2	1931 (w)	1686 (m)

^{a}([Complex] = ~10 mM, [NBu$_4$][PF$_6$] = 0.1 M in CH$_2$Cl$_2$, W.E. and C.E. Pt, and R.E. Ag/Ag$^+$).

The spin density plots for the *para*-isomers of the monocationic species $p\text{-}1^+$ reveal the full and symmetrical charge-delocalization over the Ru−C≡C−C$_6$H$_4$−C≡C−Ru linkages (Figure 12), suggesting the class III nature. On the other hand, the spin density of the *meta*-isomers $m\text{-}1^+$ is substantially localized on one of the two ruthenium fragments, as is consistent with the charge-localized class II behavior. The spin density distribution is similar to those of $p/m\text{-}5^+$, indicating again that the acyl substituents do not strongly influence the charge delocalization.

TD-DFT analysis of 1^+ shows that the lowest energy bands arise from the transitions from β-HOSOs (the highest occupied spin orbitals) to β-LUSOs (the lowest unoccupied spin orbitals) (Figure 13 and Table 6). The computed energies well coincide with the experimental data, although the sub-bands (bands B and C) of *para*-isomers 1^+ cannot be reproduced because different rotational isomers may be present.[20] For the *para*-isomers $p\text{-}1a,b^+$, both of the β-HOSO and β-LUSO show the fully delocalized Ru−C≡C−C$_6$H$_4$−C≡C−Ru character, which is in accord with the

assignment as a class III IVCT transition. On the other hand, the β-HOSOs and β-LUSOs of $m\text{-}1a,b^+$ show clear charge-transfer characters from the dπ and pπ orbitals located on one of the Ru−C≡C−C$_6$H$_4$ fragments to those on the other metal fragment. These transition characters can be assignable to typical class II type IVCT bands. On the basis of the TD-DFT results and the assignment of the lowest energy band to the IVCT bands, the V_{ab} values of $p\text{-}1a^+$, $p\text{-}1b^+$, and $m\text{-}1a^+$ estimated from the Marcus−Hush two state model are 3145 ($p\text{-}1a^+$), 3100 ($p\text{-}1b^+$) and 288 cm^{-1} ($m\text{-}1a^+$).[35−37]

ESR Study

ESR spectroscopy is another powerful tool to obtain environmental information of an unpaired electron on radical species such as the monocationic species, which was generated by in situ oxidation of the neutral species by the addition of [FeCp$_2$](PF$_6$) in CH$_2$Cl$_2$ and was subjected to the measurements as glasses after immediate freezing at 77 K (Figure 14). While intense and broadened isotropic or partially anisotropic signals with no hyperfine splitting were observed for the *para*-isomers $p\text{-}1^+$,[38] very weak signals were found for $m\text{-}1^+$. This suggests for $p\text{-}1^+$ that the unpaired electrons are delocalized over the bridging ligands on the timescale of ESR spectroscopy (~10^{-8} s). The spectra are in contrast to that observed for [Cp*(dppe)Ru−C≡C−C$_6$H$_5$]$^+$ 7^+ with a rhombic g-tensor and an isotropic g value ($g_{iso} = g_1 + g_2 + g_3$) of 2.09.[39] The g values of $p\text{-}1^+$ (~2.06) are smaller than that of 7^+ but much larger than those of organic free radicals ($g = 2.0023$). These factors further support the charge-delocalization over the Ru−C≡C−C$_6$H$_4$−C≡C−Ru moieties in $p\text{-}1^+$.

Effects of Substituents on the Cp Ligands

As expected, strong metal−metal interactions are observed for the *para*-isomers $p\text{-}1^{n+}$ as judged by their K_C, V_{ab}, and k_{et} values, which are significantly larger than those of the *meta*-isomers $m\text{-}1^{n+}$ with the different connectivities at the central benzene ring. Furthermore, the electrochemical and spectroscopic features of the core parts of the Ru complexes with/without the acyl functional groups are virtually the same. In fact, the theoretical DFT and TD-DFT studies support that the charge-delocalization properties are not perturbed by the Cp^R ligands so much when compared to the nonsubstituted Cp derivatives, although redox potential is sensitive to the electron-withdrawing substituents. Thus, these results support that Cp^R ligands (R = COOMe, COMe) can be used to evaluate the electronic structure of MV complexes without drastic electronic perturbation.
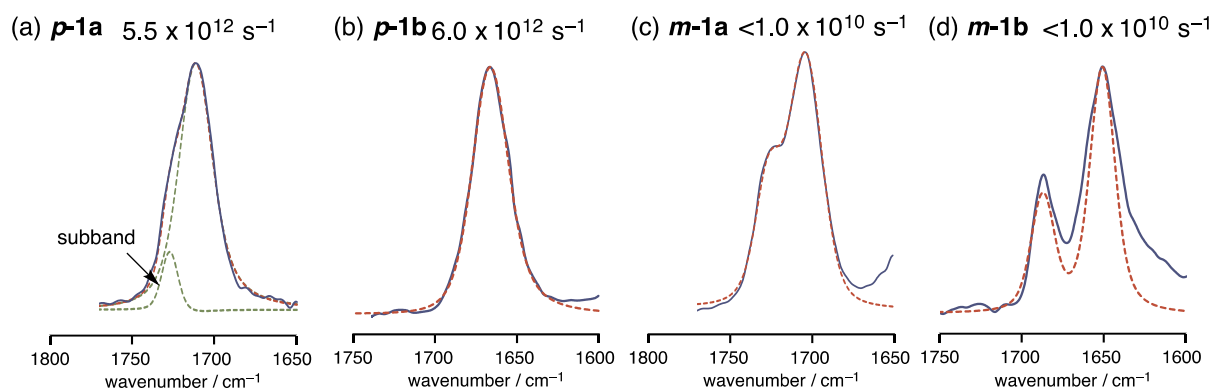
Figure 6. Experimental and simulated IR spectra [$\nu(C{=}O)$ region] for 1^+ (red dashed lines: the sum of the simulated curves, green dashed lines: individual simulated curves, and blue lines; experimentally obtained curves).
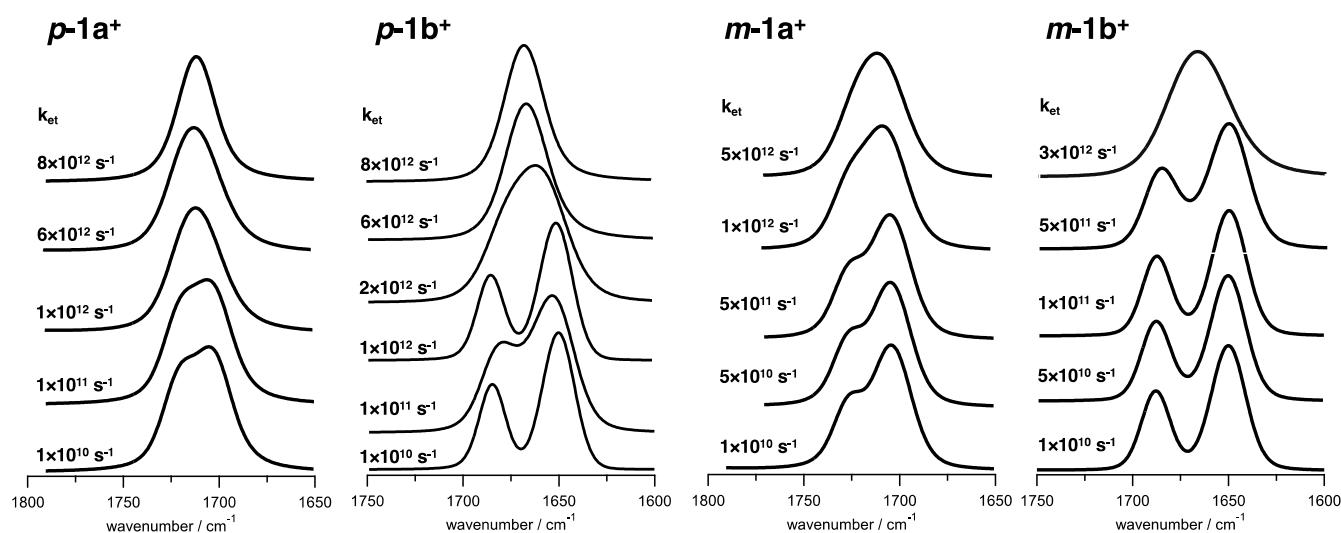
Figure 7. Band shape analysis of the $\nu(C{=}O)$ stretching vibrations for $\mathbf{1}^+$.
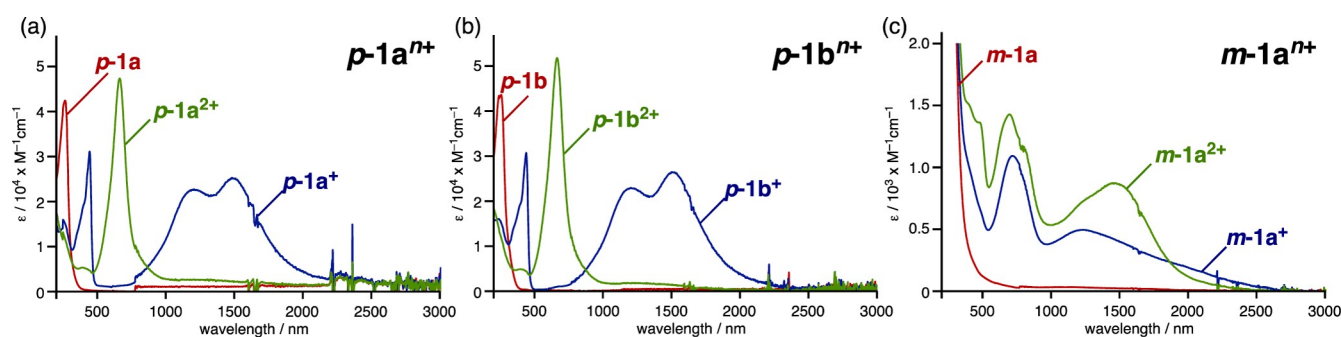
Figure 8. UV−vis−NIR spectra of (a) $p\text{-}\mathbf{1a}^{n+}$, (b) $p\text{-}\mathbf{1b}^{n+}$, and (c) $m\text{-}\mathbf{1a}^{n+}$ ($n = 0-2$) obtained with an OTTLE cell ($[p\text{-}\mathbf{1a/b}] = \sim0.1$ mM, $[m\text{-}\mathbf{1a}] = \sim1$ mM, $[\text{NBu}_4][\text{PF}_6] = 0.1$ M in CH_2Cl_2, W.E. and C.E. Pt, and R.E. Ag/Ag^+).

Table 4. UV−Vis−NIR Data for $p\text{-}\mathbf{1}^{n+}$ and $m\text{-}\mathbf{1a}^{n+}$ ($n = 0-2$) Obtained with an OTTLE Cell[a]

compound	absorption maxima/nm ($\varepsilon \times 10^{-4}/\text{cm}^{-1}\,\text{M}^{-1}$)
$p\text{-}\mathbf{1a}$	356 (4.14)
$p\text{-}\mathbf{1a}^+$	530 (3.00), 1242 (2.12), 1542 (2.37),
$p\text{-}\mathbf{1a}^{2+}$	742 (4.33)
$p\text{-}\mathbf{1b}$	348 (4.28)
$p\text{-}\mathbf{1b}^+$	532 (3.01), 1266 (2.23), 1564 (2.58)
$p\text{-}\mathbf{1b}^{2+}$	750 (4.83)
$m\text{-}\mathbf{1a}$	298 (3.11)
$m\text{-}\mathbf{1a}^+$	796 (0.197), 1326 (0.127)
$m\text{-}\mathbf{1a}^{2+}$	756 (0.305), 1460 (0.208)

[a]$[p\text{-}\mathbf{1a/b}] \sim 1$ mM, $[m\text{-}\mathbf{1a}] = \sim10$ mM, $[\text{NBu}_4][\text{PF}_6] = 0.1$ M in CH_2Cl_2, W.E. and C.E. Pt, and R.E. Ag/Ag^+.

Charge Distribution Parameter $\Delta\rho$

The charge distribution parameter, $\Delta\rho$, which was first introduced by Geiger and Gleiter, provides a degree of charge delocalization between two IR-active centers in mixed valence species (MV) of a compound $\times$ [$2{\cdot}\mathbf{X}(\text{MV}) \rightleftarrows \mathbf{X}^+(\text{ox}) + \mathbf{X}^-$ (red)].[12] $\Delta\rho$ is defined by eq 1

$$\Delta\rho = (\Delta\nu_{\text{ox}} + \Delta\nu_{\text{red}})/2(\nu_{\text{ox}} - \nu_{\text{red}}) \qquad (1)$$

where $\Delta\nu_{\text{ox}} = \nu_{\text{ox}} - \nu_{\text{ox}}^{\text{MV}}$, $\Delta\nu_{\text{red}} = \nu_{\text{red}} - \nu_{\text{red}}^{\text{MV}}$. In the present IR system, ν_{ox} and ν_{red} represent vibrational frequencies of the di-oxidized and neutral species, respectively, and $\nu_{\text{ox}}^{\text{MV}}$ and $\nu_{\text{red}}^{\text{MV}}$

represent those of the higher-energy and lower-energy bands of the mono-oxidized species, respectively (Figure 15). When $\Delta\rho = 0$ or 0.50, the complex is a localized class I species or a delocalized class III species, respectively. A compound with an intermediate $\Delta\rho$ value ($0 < \Delta\rho < 0.50$) is categorized into class II. According to the equation, the p-isomers $p\text{-}\mathbf{1a,b}^+$ with $\Delta\rho = 0.50$ turned out to be class III species, whereas the m-isomer $m\text{-}\mathbf{1a}^+$ with $\Delta\rho = 0.06$ is characterized as a class II species and the charge is localized on one of the two metal fragments (Table 7). Due to the overlapped bands for $m\text{-}\mathbf{1b}^+$, its $\Delta\rho$ value cannot be determined accurately, but the value appears to be comparable to that of $m\text{-}\mathbf{1a}^+$. When the $\Delta\rho$ values are compared to the spin densities at the Ru atoms obtained by the DFT calculations (see above), they are well consistent with the charge distribution estimated by the $\Delta\rho$ values. Thus, the IR-tag serves as a practical indicator of charge delocalization over MV species.

Comparison of k_{et} and V_{ab} Values

Electron transfer rates of MV complexes are sensitive to the environments. As the rate of solvent reorientation timescale is considered to be in the range from 10^{-11} to 10^{-12} s, IVCT bands of class II species should be affected by the polarity of the solvent. Therefore, k_{et} of class II and class III species falls below ($<10^{-11}$ s) and above ($>10^{-12}$ s) this range, respectively. As discussed above, the NIR bands of the $para$-isomers $p\text{-}\mathbf{1}^+$ showed little dependence on the solvents, and their k_{et} values
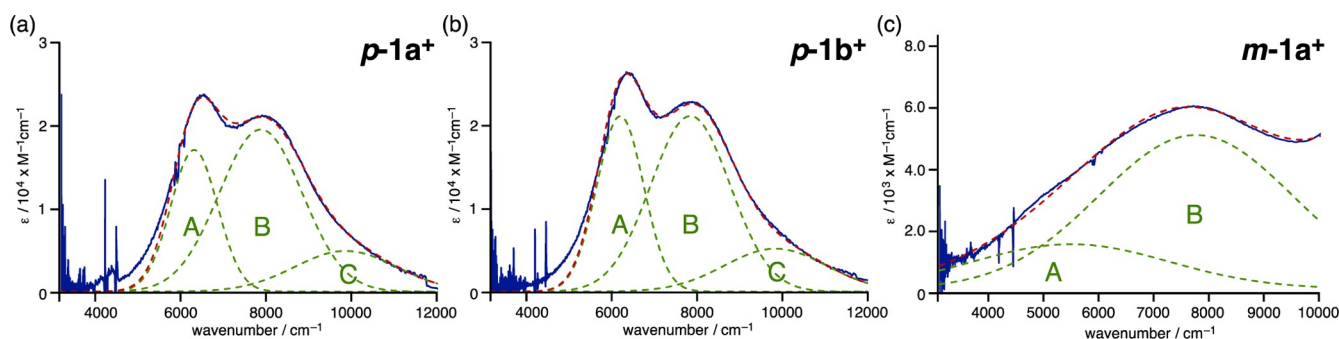
Figure 9. NIR spectra of (a) p-$1a^{n+}$, (b) p-$1b^{n+}$, and (c) m-$1a^{n+}$ obtained with an OTTLE cell and their deconvoluted spectra ($[p$-$1a/b] = \sim1$ mM, $[m$-$1a] = \sim10$ mM, $[NBu_4][PF_6] = 0.1$ M in CH_2Cl_2, W.E. and C.E. Pt, and R.E. Ag/Ag$^+$).

Table 5. NIR Spectral Data for p-1^+ and m-$1a^+$ and Related Data[a]

compound	band	ν_{max}/cm^{-1}	ε_{max}/M^{-1} cm^{-1}	$\nu_{1/2}^{calc\,b}$/cm^{-1}	ε/M^{-1} cm^{-1}	V_{ab} (classIII)[c]/V_{ab} (classII)[d]/cm^{-1} (d_{Ru-Ru})
		deconvoluted IVCT bands				
p-$1a^+$	A	6290	17050	1100	3812	3145/585
	B	7857	19521	1956	4260	3929/932
	C	9851	4878	2400	2355	4926/573
p-$1b^+$	A	6200	21138	1100	3784	3100/646
	B	7850	21156	1871	4258	3925/949
	C	9851	5184	2400	2355	4926/591
m-$1a^+$	A	5500	1457	3560	3564	288 (12.1 Å)[e], 323 (10.8 Å)[f]
	B	7760	5015	3500	4234	623 (12.1 Å)[e], 698 (10.8 Å)[f]

[a]$[p$-$1a/b] = \sim1$ mM, $[m$-$1a] = \sim10$ mM, $[NBu_4][PF_6] = 0.1$ M in CH_2Cl_2, W.E. and C.E. Pt, and R.E. Ag/Ag$^+$. [b]$\nu_{1/2}^{calc} = (2310 \times \nu_{max})^{1/2}$. [c]$V_{ab}$(class III) $= \nu_{max}/2$. [d]V_{ab}(class II) $= 2.06 \times 10^{-2} \times (\nu_{max}\,\varepsilon_{max}\,\nu_{1/2})/d_{Ru-Ru}$. [e]Through bond distances. [f]Through space distances.
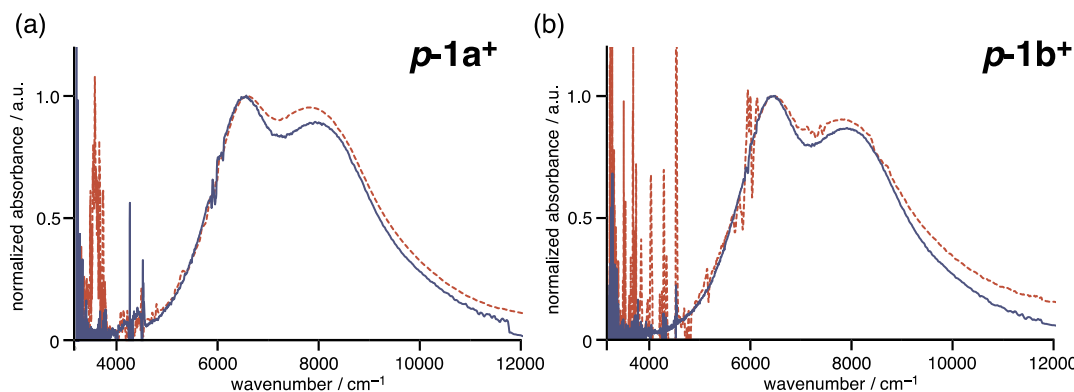
Figure 10. Normalized NIR spectra of (a) p-$1a^+$ and (a) p-$1b^+$ observed in CH_2Cl_2 (solid blue lines) and a mixed solvent of acetone/CH_2Cl_2 (98:2) (dashed red lines).

turned out to be $\sim6 \times 10^{12}$ s^{-1}, supporting their class III nature.

On the other hand, the k_{et} values of the *meta*-isomers m-1^+ are less than 10^{10} s^{-1} in accord with the assignment as class II classification. For a weakly coupled class II system, the k_{et} value can also be evaluated by using the following equations in case the electronic coupling V_{ab} is small and the thermal ET process passes through the diabatic regime.[40]

$$\Delta G^* = (\nu_{max} - 2V_{ab})^2/4\nu_{max} \qquad (2)$$

$$k_{et} = (2V_{ab}^2/h)(\pi^3/\nu_{max}k_B T)^{1/2} \exp{-(\Delta G^*/k_B T)} \qquad (3)$$

where ΔG^* is the free energy of activation needed for the thermally induced ET transfer, ν_{max} is the energy of the IVCT transition band at the maximum extinction coefficient, h is Planck's constant, k_B is Boltzmann's constant, and T is the temperature. On the basis of eqs 2 and 3, ΔG^* and k_{et} for m-$1a^+$ are determined to be 1100 cm^{-1} and 1.26×10^{11} s^{-1}, respectively. The k_{et} value is overestimated by an order of magnitude compared to that obtained by the IR methods ($<1.0 \times 10^{10}$ s^{-1}). The deviation may derive from (i) the erroneous estimation of V_{ab} values, which are determined by the deconvolution analysis of overlapped bands, (ii) the ground-state energy curves deviating from the ideal diabatic states, or (iii) the presence of rotamers as discussed above.

Scope and Limitation of the IR-Tag Strategy on the Cp Ligand

As we have discussed above, the application of the IR-tags strategy toward organometallic MV complexes with Cp ligands is useful, especially, for the estimation of the local charges on the metal fragments and of the k_{et} values obtained by the digital simulations. On the other hand, the following limitation
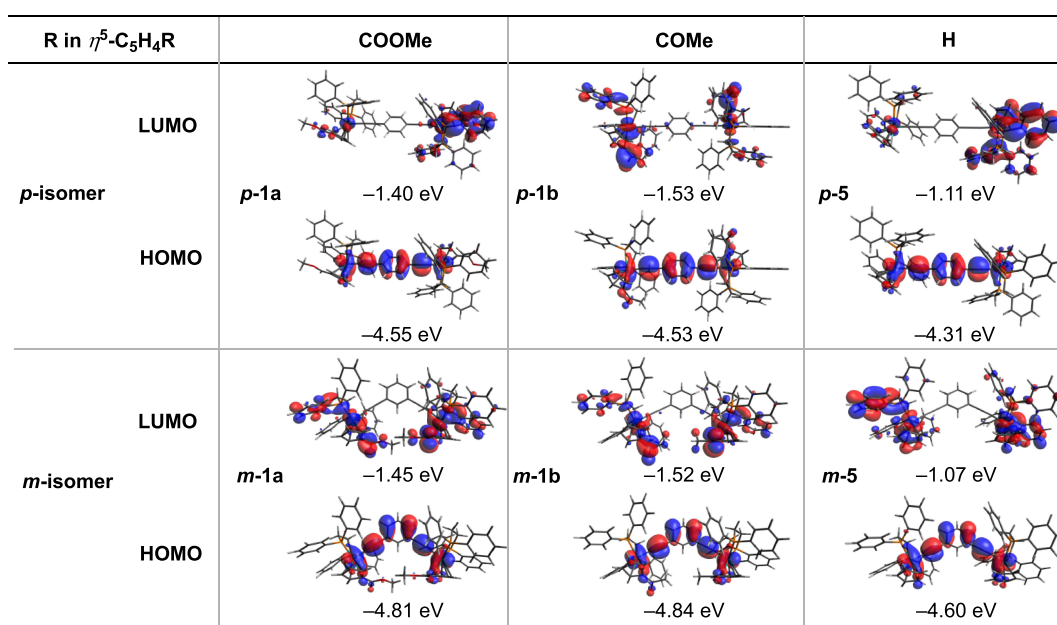
Figure 11. Frontier orbitals of *p*-**1a/b**, *m*-**1a,b**, and *p/m*-**5** and their energies.
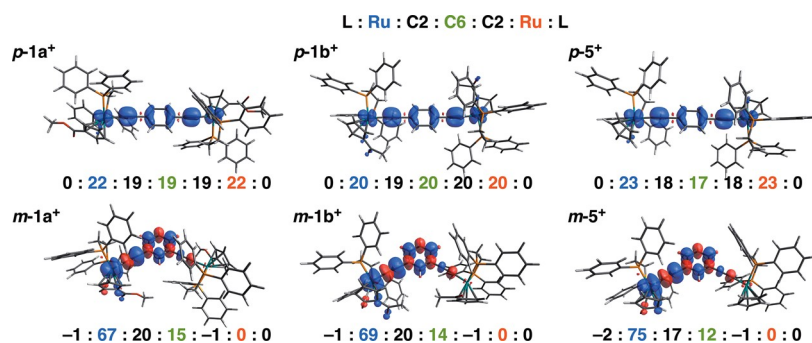
Figure 12. Spin density plots of *p*-**1**$^+$, *m*-**1**$^+$, and *p/m*-**5**$^+$. The α and β spin densities are represented in blue and red, respectively.
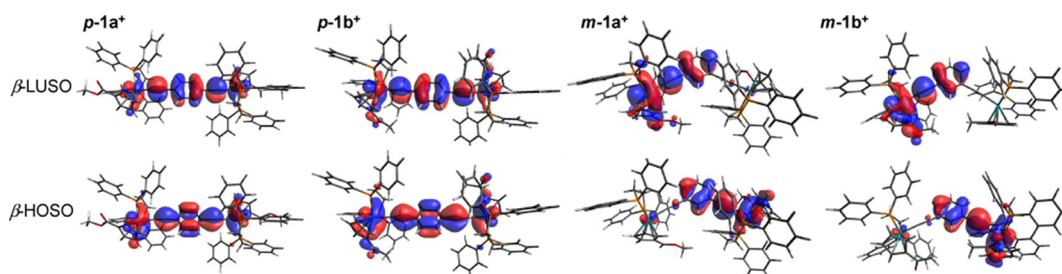
Figure 13. β-HOSO and β-LUSO orbitals for **1**$^+$.

Table 6. TD−DFT Data of NIR Bands for 1$^+$

complex	ν_{max}^{exp}/cm^{-1}	ν_{max}^{DFT}/cm^{-1} (nm)	oscillator strength	main transition	assignment
p-**1a**$^+$	6290	5435 (1840)	1.0929	β-HOSO → β-LUSO (∼100%)	IVCT
p-**1b**$^+$	6200	5714 (1750)	1.035	β-HOSO → β-LUSO (∼100%)	IVCT
m-**1a**$^+$	5500	4675 (2135)	0.0523	β-HOSO → β-LUSO (74%)	IVCT
	7760	5167 (1913)	0.0031	β-HOSO − 3 → β-LUSO (40%) β-HOSO − 4 → β-LUSO (25%)	dπ−dπ transition (ligand field)
m-**1b**$^+$		5000 (2000)	0.0118	β-HOSO − 3 → β-LUSO (70%)	dπ−dπ transition (ligand field)
		6897 (1450)	0.0579	β-HOSO → β-LUSO (89%)	IVCT

was noted in this study. The k_{et} values can be determined only when the values are within the range that the simulation allows

(10^{-10} to 10^{-12} s). Furthermore, in some case, the C=O vibrational bands can be overlapped with the other bands to
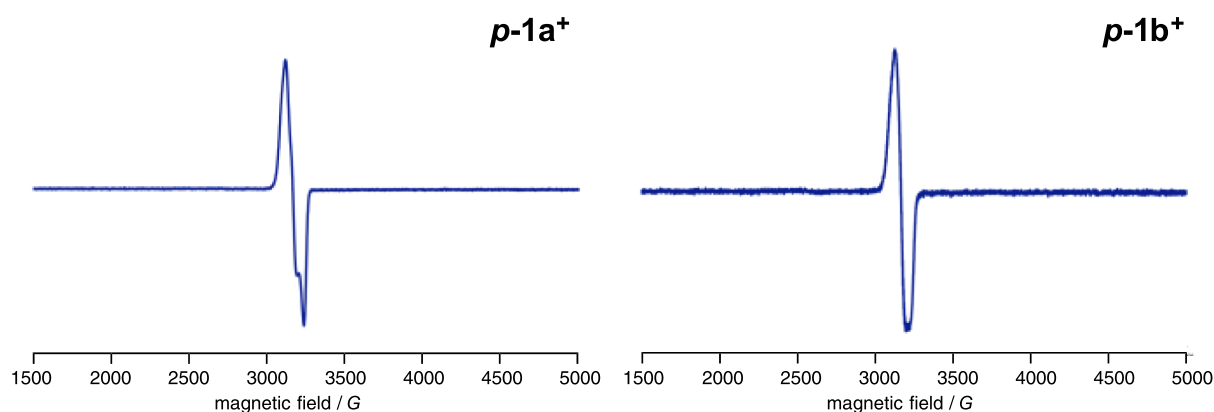
Figure 14. ESR spectra of *p*-1a⁺ and *p*-1b⁺ recorded as CH_2Cl_2 glasses at 77 K.
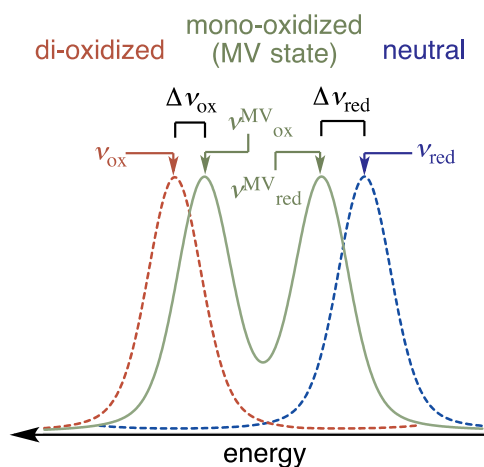
Figure 15. Schematic representation of IR stretching vibrations of a mixed valence system $[2 \cdot X(MV) \rightleftarrows X^+(ox) + X^- (red)]$.

hamper the analysis. Nevertheless, the present IR-tag method is promising because it can be facilely applied to MV complexes with various types of metal species, Cp ligands, and supporting ligands.

CONCLUSIONS

We have synthesized mono- and di-ruthenium alkynyl complexes with cyclopentadienyl ligands bearing the IR-active acyl groups and examined their electronic structures by electrochemical, spectroelectrochemical UV−vis−NIR and IR, ESR, and theoretical methods. It is clear that the *para*-isomers *p*-1 show metal−metal interactions stronger than the meta-isomers *m*-1. In contrast to the determination process of the V_{ab} value involving ambiguous factors, k_{et} can be unambiguously determined by the line shape analysis of IR spectra of the acylated Cp ligands attached to the metal centers and thus helps us fully understand the whole pictures of the

electronic structures of the metal parts in MV states. The $\nu(C{=}O)$ frequencies of the acyl groups are sensitive to the electron densities at the metal centers and, thus, afford information on the extent of charge-delocalization. As described herein, we have successfully extended the IR-tag technique toward metal alkynyl MV complexes with half-sandwich cyclopentadienyl structural motifs, which have been extensively studied for these 3 decades. This study should provide new insights into the electronic structures of metal alkynyl MV complexes.

EXPERIMENTAL SECTION

Instruments

NMR spectra were recorded on Bruker biospin AVANCE III 400 MHz (¹H 400 MHz for 2D NMR measurements) and Bruker biospin ASCEND-500 spectrometers (¹H 500 MHz, ³¹P 202 MHz ¹³C NMR 126 MHz) in $CDCl_3$. NMR chemical shifts were referenced to the residual protio impurities in the deuterated solvents. ESI-TOF-MS analysis was performed on a Bruker micrOTOF II spectrometer. UV−vis and IR spectra (KBr pellets and CH_2Cl_2 solution) were recorded on JASCO V670DS and FTIR 4200 spectrometers, respectively. Electrochemical measurements (CV and DPV) were made with a Hokuto Denko HZ-5000 [observed in CH_2Cl_2; [complex] = *ca.* 1 × 10⁻³ M; [NBu₄PF₆] = 0.1 M; working electrode: Pt, counter electrode: Pt, reference electrode: Ag/AgNO₃; and scan rate was 100 mV/s (CV)]. After the measurement, ferrocene (Fc) was added to the mixture and the potentials were calibrated with respect to the Fc/Fc⁺ redox couple. ESR spectra for the monocationic species were recorded on a JEOL JES-FA100 spectrometer, and samples were prepared by the addition of small amounts of oxidant [tris(4-bromophenyl)aminium hexachloroantimonate] to CH_2Cl_2 solutions of the complexes in ESR tubes under a N_2 atmosphere just before cooling in a liquid nitrogen bath. The spectra were recorded at the liquid nitrogen temperature. X-ray crystal analysis was performed on a Bruker Smart Apex II Ultra diffractometer. CCDC numbers 1861281−1861286 contain the supplementary crystallographic data for *p*-1a (1861281), *p*-1b (1861282), *m*-1a (1861283), *m*-1b (1861284), 2a (1861285), and 2b (1861286).

Table 7. Parameters Derived from IR, UV−Vis−NIR, and DFT Studies

compound	$\Delta\nu_{ox}$/cm⁻¹	$\Delta\nu_{red}$/cm⁻¹	$\nu_{ox} - \nu_{red}$	$\Delta\rho^a$	charge distribution on the two metal centers (%)	spin densities at the two metal centers[b] (%)	ΔG^*/cm⁻¹	k_{et}/s⁻¹
p-1a⁺	9	15	24	0.50	50:50	50:50		6 × 10¹²
p-1b⁺	16	18	34	0.50	50:50	50:50		6 × 10¹²
m-1a⁺	1	2	25	0.06	94:6	100:0	1100	<1.0 × 10¹⁰
m-1b⁺	1	0	36	*c*	*c*	100:0		<1.0 × 10¹⁰

$^a\rho = (\Delta\nu_{ox} + \Delta\nu_{ox})/0.5(\nu_{ox} - \nu_{red})$. [b]Estimated from the DFT calculations. [c]Not determined due to overlapped bands.

Spectroelectrochemistry

All measurements were conducted under a N_2 atmosphere. Spectroelectrochemical UV−vis−NIR measurements were performed in a home-built 1 mm quartz cell equipped with working (Pt mesh), counter (Pt wire), and reference electrodes (Ag/AgNO$_3$). A CH_2Cl_2 solution of complex (0.1 mM for *p*-**1a,b**, 1 mM for *m*-**1a,b**) was subjected to the measurements in the presence of NBu$_4$PF$_6$ (0.1 M), a supporting electrolyte. The spectroelectrochemical IR measurements were performed with an OTTLE cell, purchased from the University of Reading, which comprised a Pt-mesh working and counter electrodes and a thin silver wire as a pseudo-reference electrode. The optical beam was passed through CaF$_2$ windows of a conventional liquid IR cell. The conditions were the same as those for the spectroelectrochemical UV−vis−NIR measurements except the concentration of the complexes (10 mM for **1**).

Materials

Reactions were performed under a N_2 atmosphere using the standard Schlenk tube technique unless stated otherwise. Purchased dry THF, CH_2Cl_2, and hexane were further purified by the Grubbs solvent purification system.[41] Dry acetone purchased from Kanto Chemical Co., Inc. was used without further purification. Triethylamine was predried over KOH pellets and distilled from CaH$_2$. DBU was distilled from CaH$_2$. Other regents, silica gel (Kanto chemical Co Inc. Silica Gel 60N), and alumina (Merck Aluminum oxide 90 standardized) were used as received. RuCl$_2$(PPh$_3$)$_3$,[42] sodium methoxycarbonylcyclopentadienide,[24] and sodium acetylcyclopentadienide[24] were synthesized according to the literature procedures.

Synthesis of 3a. A THF (50 mL) solution of RuCl$_2$(PPh$_3$)$_3$ (3.00 g, 3.13 mmol) and sodium methoxycarbonylcyclopentadienide (487 mg, 3.33 mmol) was stirred for 1 h at room temperature. The mixture was concentrated and hexane (80 mL) was added to form red precipitates, which were collected by filtration, washed with hexane, and dried under reduced pressure to afford crude products of **3a**. To the obtained solid was added dppe (1.247 g, 3.13 mmol) and toluene (50 mL), and the mixture was refluxed for 4 h. After the mixture was cooled to room temperature, the volatiles were evaporated, and the resulting solid was subjected to silica gel column chromatography (CH$_2$Cl$_2$/Et$_2$O = 9:1) to yield **3a** (824 mg, 1.25 mmol, 40%) as a yellow powder. ^{1}H NMR: δ 7.83−7.76 (m, 4H, Ph in dppe), 7.40−7.36 (m, 6H, Ph), 7.33−7.26 (m, 6H, Ph), 7.12 (virtual t, J = 8.7 Hz, 4H, Ph), 5.24 (t, J = 2.0 Hz, 2H, η^5-C$_5$H$_4$-R), 4,14 (t, J = 2.0 Hz, 2H, η^5-C$_5$H$_4$-R), 3.60 (s, 3H, COOCH$_3$), 2.78−2.61 (m, 2H, CH$_2$), 252−2.35. (m, 2H, CH$_2$). ^{31}P NMR: δ 79.1 (s). ^{13}C{^{1}H} NMR: δ 167.8 (s, COOMe) 140.5 (virtual dt, J_{C-P} = 43.6, 12.9 Hz, ipso-Ph in dppe), 134.2 (t, J_{C-P} = 4.9 Hz, o-Ph in dppe), 134.5−133.8 (m, ipso-Ph in dppe), 131.7 (t, J_{C-P} = 4.8 Hz, o-Ph in dppe), 130.0 (s, p-Ph in dppe), 129.5 (s, p-Ph in dppe-Ph), 128.3 (t, J_{C-P} = 4.4 Hz, m-Ph in dppe), 128.1 (t, J_{C-P} = 4.7 Hz, m-Ph in dppe), 89.1, 79.7, 76.7 (s × 3, η^5-C$_5$H$_4$-R), 51.5 (s, COOMe), 27.5 (m, CH$_2$ in dppe). HRESI-TOF MS (m/z): calcd for C$_{33}$H$_{31}$P$_2$O$_2$Ru, 623.0846. Found: 623.0845 [M−Cl]$^+$. IR(KBr/cm^{-1}): 1705 ν(C=O). Anal. Calcd for C$_{32.1}$H$_{31.2}$Cl$_{1.2}$O$_2$P$_2$Ru (**3a**·(CH$_2$Cl$_2$)$_{0.1}$): C, 58.90; H, 4.80. Found: C, 59.02; H, 4.28.

Synthesis of 3b. Synthesis of **3b** was previously reported,[24] but we prepared **3b** in a manner analogous to the synthesis of **3a** using RuCl$_2$(PPh$_3$)$_3$ (3.00 g, 3.13 mmol), sodium acetylcyclopentadienide (429 mg, 3.30 mmol), and dppe(1.247 g, 3.13 mmol). **3b** was obtained as a yellow powder (987 mg, 1.54 mmol, 49%). The spectral data were consistent with the value reported previously. ^{1}H NMR: δ 7.74−7.68 (m, 4H, o-Ph in dppe), 7.42−7.38 (m, 6H, Ph), 7.34 (t, J = 7.3 Hz, 2H, Ph), 7.30 (t, J = 7.3 Hz, 4H, Ph), 7.12 (virtual t, J = 8.0 Hz, 4H, o-Ph in dppe), 5.30 (m, 2H, η^5-C$_5$H$_4$-R), 4.18−4.10 (m, 2H, η^5-C$_5$H$_4$-R), 2.78−2.60 (m, 2H, CH$_2$ in dppe), 2.42−2.23 (m, 2H, CH$_2$ in dppe), 1.95 (s, 3H, COCH$_3$). ^{31}P NMR: δ 78.2 (s).^{13}C{^{1}H} NMR: δ 196.5 (s, COMe), 139.5 (virtual dt, J_{C-P} = 43.8, 12.6 Hz, ipso-Ph in dppe), 133.6 (t, J_{C-P} = 5.0 Hz, o-Ph in dppe), 131.8 (t, J_{C-P} = 5.0 Hz, o-Ph in dppe), 129.9 (s, p-Ph in dppe), 129.7 (s, p-Ph in dppe), 128.2 (t, J_{C-P} = 4.8 Hz, m-Ph in dppe), 127.9 (t, J_{C-P} = 5.0 Hz,

m-Ph in dppe), 88.4, 88.0, 76.7 (s × 3, η^5-C$_5$H$_4$-R), 28.2 (s, COMe), 26.7 (m, CH$_2$ in dppe). IR(KBr/cm^{-1}): 1653 ν(C=O).

General Procedure for the Synthesis of Alkynylruthenium Complexes

To a mixture of Cp^{R}RuCl(dppe) (1 equiv, 0.15−0.5 mmol scale) and AgBF$_4$ (1 equiv) was added CH_2Cl_2 (5−10 mL), and the resultant mixture was stirred at room temperature for 30 min. The suspension was filtered through a Celite pad to remove precipitated AgCl and the filtrate was added to a solution of the appropriate ethynylbenzene (1 and 0.5 equiv for mono- and di-nuclear complexes, respectively) in CH_2Cl_2 (5−10 mL). After the mixture was stirred for 1 h, several drops of DBU (<∼50 μL) was added to the reaction mixture, which was further stirred for 1 h. The solution was evaporated and the obtained residue was subjected to silica gel column chromatography (CH$_2$Cl$_2$) to afford the product.

Synthesis of 2a. The title complex was obtained from **3a** (100 mg, 0.152 mmol) and 4-ethynyltoluene (17 mg, 0.15 mmol) as a yellow powder (83 mg, 0.11 mmol, 74%). ^{1}H NMR: δ 7.89−7.83 (m, 4H, o-Ph in dppe), 7.42−7.37 (m, 6H, Ph), 7.34−7.21 (m, 10H, Ph), 6.74 (d, 2H, J = 7.9 Hz, C$_6$H$_5$CH$_3$), 6.39 (d, 2H, J = 7.9 Hz, C$_6$H$_5$CH$_3$), 5.49 (t, J = 2.2 Hz, 2H, η^5-C$_5$H$_4$-R), 4.60 (t, J = 2.2 Hz, 2H, η^5-C$_5$H$_4$-R), 3.48 (s, 3H, C(O)OCH$_3$), 2.80−2.63 (m, 2H, CH$_2$ in dppe), 2.40−2.23 (virtual octet, J = 6.8 Hz, 2H, CH$_2$ in dppe), 2.18 (s, 3H, C$_6$H$_5$CH$_3$). ^{31}P NMR: δ 85.0 (s). ^{13}C{^{1}H} NMR: δ 167.5 (s, COMe), 141.6 (virtual dt, J_{C-P} = 39.2, 9.2 Hz, ipso-Ph in dppe), 136.2 (virtual td, J_{C-P} = 27.4, 4.6 Hz, ipso-Ph in dppe), 134.2 (t, J = 5.1 Hz, o-Ph in dppe), 132.9 (s, C$_6$H$_5$CH$_3$), 131.8 (t, J_{C-P} = 5.1 Hz, o-Ph in dppe), 130.4 (s, C$_6$H$_5$CH$_3$), 129.6 (s, p-Ph in dppe), 129.2 (s, p-Ph in dppe), 128.2 (s, C$_6$H$_5$CH$_3$), 128.1 (t, J = 4.7 Hz, m-Ph in dppe), 127.7 (t, J = 5.0 Hz, m-Ph in dppe), 126.9 (s, C$_6$H$_5$CH$_3$), 111.7 (s, Ru−C≡C), 111.0 (t, J = 25.7 Hz, Ru−C≡C), 89.3, 83.0, 82.4 (s × 3, η^5-C$_5$H$_4$-R), 51.2 (s, COOMe), 28.4 (m, CH$_2$ in dppe), 21.2 (s, C$_6$H$_5$CH$_3$). HRESI-TOF MS (m/z): calcd for C$_{42}$H$_{38}$P$_2$O$_2$Ru, 738.1397. Found: 738.1397 [M]$^+$. IR(CH$_2$Cl$_2$/cm^{-1}): 2085 ν(C≡C), 1703 ν(C=O). Anal. Calcd for C$_{42}$H$_{38}$O$_2$P$_2$Ru: C, 68.38; H, 5.19. Found: C, 68.38; H, 5.24.

Synthesis of 2b. The title complex was obtained from **3b** (100 mg, 0.156 mmol) and 4-ethynyltoluene (17 mg, 0.15 mmol) as a yellow powder (63 mg, 0.087 mmol, 58%). ^{1}H NMR: δ 7.77−7.71 (m, 4H, o-Ph in dppe), 7.42−7.38 (m, 6H, Ph), 7.33 (t, J = 7.7 Hz, 2H, p-Ph in dppe), 7.28 (t, J = 7.0 Hz, 4H, Ph), 7.23 (m, 4H, Ph), 6.80 (d, J = 7.8 Hz, 2H, C$_6$H$_5$CH$_3$), 6.47 (d, J = 7.8 Hz, 2H, C$_6$H$_5$CH$_3$), 5.54 (t, J = 2.1 Hz, 2H, η^5-C$_5$H$_4$-R), 4.56−4.52 (m, 2H, η^5-C$_5$H$_4$-R), 2.80−2.66 (m, 2H, CH$_2$ in dppe), 2.30−2.13 (m, 2H, CH$_2$ in dppe), 2.21 (s, 3H, C$_6$H$_5$CH$_3$), 1.95 (s, 3H, COCH$_3$). ^{31}P NMR: δ 83.9 (s).^{13}C{^{1}H} NMR: δ 196.1 (s, COMe), 140.6 (virtual dt, J_{C-P} = 34.4, 11.1 Hz, ipso-Ph in dppe), 135.7 (virtual td, J_{C-P} = 26.2, 5.4 Hz, ipso-Ph in dppe), 133.5 (t, J_{C-P} = 4.9 Hz, o-Ph in dppe), 133.3 (s, C$_6$H$_5$CH$_3$), 132.0 (t, J_{C-P} = 5.3 Hz, o-Ph in dppe), 130.3 (s, C$_6$H$_5$CH$_3$), 129.4 (s, p-Ph in dppe), 129.3 (s, p-Ph in dppe), 128.2 (s, C$_6$H$_5$CH$_3$), 128.0 (t, J_{C-P} = 4.7 Hz, m-Ph in dppe), 127.5 (t, J_{C-P} = 5.0 Hz, m-Ph in dppe), 126.7 (s, C$_6$H$_5$CH$_3$), 112.7 (t, J = 24.9 Hz, Ru−C≡C), 111.5 (s, Ru−C≡C), 90.3, 89.2, 82.6 (s × 3, η^5-C$_5$H$_4$-R), 27.8 (m, CH$_2$ in dppe), 27.4 (s, COMe), 21.1 (s, C$_6$H$_5$CH$_3$). HRESI-TOF MS (m/z): calcd for C$_{42}$H$_{38}$P$_2$ORu, 722.1447 [M]$^+$. Found: 722.1447 [M]$^+$. IR(CH$_2$Cl$_2$/cm^{-1}): 2085 ν(C≡C), 1650 ν(C=O). Anal. Calcd for C$_{42.3}$H$_{38.6}$Cl$_{0.6}$OP$_2$Ru (**2b**·(CH$_2$Cl$_2$)$_{0.3}$): C, 67.99; H, 5.21. Found: C, 67.77; H, 5.23.

Synthesis of *p*-1a. The title complex was obtained from **3a** (320 mg, 0.486 mmol) and 1,4-diethynylbenzene (30 mg, 0.24 mmol) as a yellow powder (245 mg, 0.179 mmol, 75%). ^{1}H NMR: δ 7.79 (virtual t, J = 8.5 Hz, m, 8H, o-Ph in dppe), 7.37−7.20 (m, 32H, Ph), 6.11 (s, 4H, C$_6$H$_4$), 5.44 (t, J = 2.1 Hz, 4H, η^5-C$_5$H$_4$-R), 4.57 (t, J = 2.1 Hz, 4H, η^5-C$_5$H$_4$-R), 3.43 (s, 3H, C(O)OCH$_3$), 2.75−2.60 (m, 4H, CH$_2$ in dppe), 2.35−2.18 (m, 4H, CH$_2$ in dppe). ^{31}P NMR: δ 84.9 (s). ^{13}C{^{1}H} NMR: δ 167.4 (s, C(O)OMe), 141.1 (virtual dt, J_{C-P} = 39.0, 9.6 Hz, ipso-Ph in dppe), 136.1 (virtual td, J_{C-P} = 28.0, 4.5 Hz, ipso-Ph in dppe), 134.0 (m, o-Ph in dppe), 131.6 (m, o-Ph in dppe), 129.3 (s, p-Ph in dppe), 129.0 (s, p-Ph in dppe), 127.9 (m, m-Ph in dppe),

127.5 (m, m-Ph in dppe), 112.7 (s, Ru$-$C$\equiv$C), 110.7 (t, J = 26.5 Hz, Ru$-$C$\equiv$C), 89.2 (s, η^5-C_5H_4-R), 83.0 (s, η^5-C_5H_4-R), 51.2 (s, C(O)OMe) 28.4 (m, CH_2 in dppe). HRESI-TOF MS (m/z): calcd for $C_{76}H_{66}P_4O_4Ru_2$, 1370.1998 $[M]^+$. Found 1370.1995 $[M]^+$. IR(CH_2Cl_2/cm^{-1}): 2085 ν(C$\equiv$C), 1703 ν(C$=$O). Anal. Calcd for $C_{76.3}H_{66.6}Cl_{0.6}O_4P_4Ru_2$ (p-$1a\cdot$ (CH_2Cl_2)$_{0.3}$): C, 65.70; H, 4.81. Found: C, 65.54; H, 4.70.

Synthesis of p-1b. The title complex was obtained from **3b** (130 mg, 0.202 mmol) and 1,4-diethynylbenzene (13 mg, 0.10 mmol) as a yellow powder (61 mg, 0.045 mmol, 45%). ^{1}H NMR: δ 7.71 (virtual t, J = 7.8 Hz, 8H, o-Ph in dppe), 7.38$-$7.25 (m, 24H, Ph), 7.20 (virtual t, J = 8.9 Hz, 8H, Ph), 6.25 (s, 4H, C_6H_4), 5.51 (t, J = 2.0 Hz, 4H, η^5-C_5H_4-R), 4.52 (s, 4H, η^5-C_5H_4-R), 2.79$-$2.60 (m, 4H, CH_2 in dppe), 2.28$-$2.11 (m, 4H, CH_2 in dppe), 1.91 (s, 6H, COCH_3) ^{31}P NMR: δ 83.9 (s). ^{13}C{^{1}H} NMR: δ 196.0 (s, COMe), 140.6 (virtual dt, J_{C-P} = 39.6, 18.6 Hz, $ipso$-Ph in dppe), 135.7 (virtual dt, J_{C-P} = 52.2, 25.6 Hz, $ipso$-Ph in dppe), 133.5 (m, o-Ph in dppe), 132.0 (m, o-Ph in dppe), 129.6$-$129.3 (m, p-Ph in dppe and C_6H_4), 128.0 (m, p-Ph in dppe), 127.5 (m, m-Ph in dppe), 124.9 (s, C_6H_4), 113.2 (t, J = 24.3 Hz, Ru$-$C$\equiv$C), 112.4 (s, C$\equiv$C), 90.3, 89.2, 82.6 (s × 3, η^5-C_5H_4-R), 27.8 (m, CH_2 in dppe), 27.4 (s, COMe) HRESI-TOF MS (m/z): calcd for $C_{76}H_{66}P_4O_2Ru_2$, 1338.2099 $[M]^+$. Found: 1338.2093 $[M]^+$. IR(CH_2Cl_2/cm^{-1}): 2081 ν(C$\equiv$C), 1650 ν(C$=$O). Anal. Calcd for $C_{77}H_{68}Cl_2O_2P_4Ru_2$ (p-$1b\cdot$ CH_2Cl_2): C, 65.02; H, 4.82. Found: C, 65.67; H, 4.70.

Synthesis of m-1a. The title complex was obtained from **3a** (160 mg, 0.243 mmol) and 1,3-diethynylbenzene (14 mg, 0.11 mmol) as a yellow powder (121 mg, 0.088 mmol, 80%). ^{1}H NMR: δ 7.80 (virtual t, J = 8.0 Hz, 8H, o-Ph in dppe), 7.32$-$7.17 (m, 32H, Ph), 6.54 (t, J = 7.7 Hz, 1H, C_6H_4), 6.20 (t, J = 1.6 Hz, 1H, C_6H_4), 6.10 (dd, J_1 = 7.7 Hz, J_2 = 1.6 Hz, 2H, C_6H_4), 5.48 (t, J = 2.2 Hz, 4H, η^5-C_5H_4-R), 4.58 (t, J = 2.2 Hz, 4H, η^5-C_5H_4-R), 3.41 (s, 6H, COOMe), 2.80$-$2.66 (virtual octet, J = 5.9 Hz, 4H, CH_2 in dppe), 2.39$-$2.24 (virtual octet, J = 5.3 Hz, 4H, CH_2 in dppe). ^{31}P NMR: δ 84.9 (s). ^{13}C{^{1}H} NMR: δ 167.4 (s, COOMe), 141.5 (virtual td, J_{C-P} = 26.9, 8.6 Hz, $ipso$-Ph in dppe), 136.4 (virtual td, J_{C-P} = 28.7, 4.3 Hz,, $ipso$-Ph in dppe), 134.0 (t, J_{C-P} = 4.9 Hz, o-Ph in dppe), 132.0 (s, C_6H_4), 131.9 (t, J_{C-P} = 5.2 Hz, o-C_6H_5 in dppe), 129.5 (s, p-C_6H_5 in dppe), 129.1 (s, p-Ph in dppe), 128.9 (s, C_6H_4), 128.1 (t, J_{C-P} = 4.5 Hz, m-Ph in dppe), 127.6 (t, J_{C-P} = 5.0 Hz, m-Ph in dppe), 126.5 (s, C_6H_4), 126.4 (s, C_6H_4), 112.4 (s, C$\equiv$C), 109.7 (t, J_{C-P} = 25.6 Hz, Ru$-$C$\equiv$C), 89.3, 83.1, 82.6 (s × 3, η^5-C_5H_4-R), 51.2 (s, COOMe), 28.5 (m, CH_2-dppe). HRESI-TOF MS (m/z): calcd for $C_{76}H_{66}P_4O_4Ru_2$, 1370.1998 $[M]^+$. Found: 1338.2003 $[M]^+$. IR(CH_2Cl_2/cm^{-1}): 2075 ν(C$\equiv$C), 1703 ν(C$=$O). Anal. Calcd for $C_{76}H_{66}O_4P_4Ru_2 \cdot 0.5(CH_2Cl_2)$: C, 65.08; H, 4.78. Found: C, 64.72; H, 4.54.

Synthesis of m-1b. The title complex was obtained from **3b** (130 mg, 0.202 mmol) and 1,3-diethynylbenzene (13 mg, 0.10 mmol) as a yellow powder (66 mg, 0.048 mmol, 48%). ^{1}H NMR: δ 7.73$-$7.67 (m, 8H, o-Ph in dppe), 7.35$-$7.24 (m, 24H, Ph), 7.19 (virtual t, J = 8.1 Hz, 8H, o-Ph in dppe), 6.62 (t, J = 7.7 Hz, 1H, C_6H_4), 6.32 (t, J = 1.6 Hz, 1H, C_6H_4), 6.16 (dd, J = 7.7 Hz, J_2 = 1.6 Hz, 2H, C_6H_4), 5.53 (t, J = 2.1 Hz, 4H, η^5-C_5H_4-R), 4.54$-$4.52 (m, 4H, η^5-C_5H_4-R), 2.82$-$2.65 (virtual octet, J = 6.3 Hz, 4H, CH_2 in dppe), 2.32$-$2.15 (virtual octet, J = 6.9 Hz, 4H, CH_2 in dppe), 1.91 (s, 6H, COCH_3). ^{31}P NMR: δ 84.1(s). ^{13}C{^{1}H} NMR: δ 195.9 (s, $-$COMe), 140.7 (virtual dt, J_{C-P} = 39.7, 18.1 Hz, $ipso$-Ph in dppe), 135.8 (virtual dt, J_{C-P} = 27.9, 5.9 Hz, $ipso$-Ph in dppe), 133.6 (t, J_{C-P} = 4.8 Hz, o-Ph in dppe), 132.0 (t, J_{C-P} = 5.2 Hz, o-Ph in dppe), 131.7 (s, C_6H_4), 129.5 (s, p-Ph in dppe), 129.4 (s, p-Ph in dppe), 128.9 (s, C_6H_4), 128.1 (t, J_{C-P} = 4.5 Hz, m-Ph in dppe), 127.6 (t, J_{C-P} = 5.0 Hz, m-Ph in dppe), 126.8 (s, C_6H_4), 126.7 (s, C_6H_4), 112.5 (t, J = 24.6 Hz, Ru$-$C$\equiv$C), 112.3 (s, C$\equiv$C), 90.4, 89.4, 82.9 (s × 3, η^5-C_5H_4-R), 28.0 (m, CH_2-dppe), 27.6 (s, COMe). HRESI-TOF MS (m/z): calcd for. $C_{76}H_{66}P_4O_2Ru_2$, 1338.2099 $[M]^+$. Found: 1338.2092 $[M]^+$. IR(CH_2Cl_2/cm^{-1}): 2074 ν(C$\equiv$C), 1650 ν(C$=$O). Anal. Calcd for $C_{76.1}H_{66.2}Cl_{0.2}O_2P_4Ru_2$ (m-**1b**$\cdot$ (CH_2Cl_2)$_{0.1}$): C, 67.91; H, 4.96. Found: C, 67.56; H, 4.75.

DFT Calculations

DFT calculations were performed by using the Gaussian 09 (D01) and 16 (A01) program packages.[43] Optimizations of geometry for the neutral and monocationic complexes were carried out with the (U)B3LYP/LanL2DZ levels of theory with CPCM (CH_2Cl_2) solvent continuum. Single-point calculations of neutral complexes were performed at the same level of theory. TD-DFT calculations and spin density plots were conducted with UBLYP35/Def2SVP with the CPCM solvent continuum of CH_2Cl_2 levels of theory.[44] We also tried geometry optimization using the UBLYP35/Def2SVP level of theory, but resulted in the charge-localized geometry for the para-isomers, which were not consistent with our experimental results.

■ ASSOCIATED CONTENT

ⓢ Supporting Information

The Supporting Information is available free of charge at https://pubs.acs.org/doi/10.1021/acsorginorgau.2c00005.

    Spectral, electrochemical, and X-ray diffraction data and Cartesian coordinates of optimized geometries (PDF)

Accession Codes

CCDC 1861281$-$1861286 contain the supplementary crystallographic data for this paper. These data can be obtained free of charge via www.ccdc.cam.ac.uk/data_request/cif, or by emailing data_request@ccdc.cam.ac.uk, or by contacting The Cambridge Crystallographic Data Centre, 12 Union Road, Cambridge CB2 1EZ, UK; fax: +44 1223 336033.

■ AUTHOR INFORMATION

Corresponding Authors

Yuya Tanaka $-$ *Laboratory for Chemistry and Life Science, Institute of Innovative Research, Tokyo Institute of Technology, Yokohama 226-8503, Japan;* ◎ orcid.org/0000-0002-0674-660X; Email: ytanaka@res.titech.ac.jp

Munetaka Akita $-$ *Laboratory for Chemistry and Life Science, Institute of Innovative Research, Tokyo Institute of Technology, Yokohama 226-8503, Japan;* ◎ orcid.org/0000-0001-7007-9621; Email: akitatit@icloud.com

Author

Hiroki Takahashi $-$ *Department of Chemical Science and Engineering, School of Materials and Chemical Technology, Tokyo Institute of Technology, Yokohama 226-8503, Japan*

Complete contact information is available at:
https://pubs.acs.org/10.1021/acsorginorgau.2c00005

Author Contributions

Y.T. and H.T. contributed equally to this work. All the experiments were conducted by H.T. Y.T. contributed to the theoretical study. The manuscript was drafted by Y.T. and edited by M.A. All authors have given approval to the final version of the manuscript.

Notes

The authors declare no competing financial interest.

■ ABBREVIATIONS

dppe 1,2-bis(diphenylphosphino)ethane
Cp   cyclopentadinyl
Cp*   1,2,3,4,5-pentamethylcyclopentadienyl
W.E   working electrode,
R.E.   reference electrode,
C.E.   counter electrode

■ REFERENCES

(1) Creutz, C.; Taube, H. Direct Approach to Measuring the Franck-Condon Barrier to Electron Transfer between Metal Ions. *J. Am. Chem. Soc.* **1969**, *91*, 3988−3989.

(2) Robin, M. B.; Day, P. Mixed Valence Chemistry-A Survey and Classification. In *Advances in Inorganic Chemistry and Radiochemistry*; Eméleus, H. J., Sharpe, A. G., Eds.; Academic Press, 1968; Vol. *10*, pp 247−422.

(3) Barrière, F.; Camire, N.; Geiger, W. E.; Mueller-Westerhoff, U. T.; Sanders, R. Use of Medium Effects to Tune the ΔE1/2 Values of Bimetallic and Oligometallic Compounds. *J. Am. Chem. Soc.* **2002**, *124*, 7262.

(4) Barrière, F.; Geiger, W. E. Use of Weakly Coordinating Anions to Develop an Integrated Approach to the Tuning of ΔE1/2 Values by Medium Effects. *J. Am. Chem. Soc.* **2006**, *128*, 3980.

(5) Hush, N. S. Distance Dependence of Electron Transfer Rates. *Coord. Chem. Rev.* **1985**, *64*, 135−157.

(6) Demadis, K. D.; Hartshorn, C. M.; Meyer, T. J. The Localized-to-Delocalized Transition in Mixed-Valence Chemistry. *Chem. Rev.* **2001**, *101*, 2655−2686.

(7) Ito, T.; Hamaguchi, T.; Nagino, H.; Yamaguchi, T.; Washington, J.; Kubiak, C. P. Effects of Rapid Intramolecular Electron Transfer on Vibrational Spectra. *Science* **1997**, *277*, 660−663.

(8) Mücke, P.; Linseis, M.; Záliš, S.; Winter, R. F. Vinyl-Ruthenium Entities as Markers for Intramolecular Electron Transfer Processes. *Inorg. Chim. Acta* **2011**, *374*, 36−50.

(9) Winter, R. F. Half-Wave Potential Splittings ΔE1/2 as a Measure of Electronic Coupling in Mixed-Valent Systems: Triumphs and Defeats. *Organometallics* **2014**, *33*, 4517−4536.

(10) Atwood, C. G.; Geiger, W. E.; Rheingold, A. L. Structural Consequences of Electron-Transfer Reactions. 26. Evidence for Time-Dependent Valence Detrapping in a Mixed-Valent Dimanganese Fulvalenyl Cation. *J. Am. Chem. Soc.* **1993**, *115*, 5310−5311.

(11) Stoll, M. E.; Lovelace, S. R.; Geiger, W. E.; Schimanke, H.; Hyla-Kryspin, I.; Gleiter, R. Transannular Effects in Dicobalta−Superphane Complexes on the Mixed-Valence Class II/Class III Interface: Distinguishing between Spin and Charge Delocalization by Electrochemistry, Spectroscopy, and Ab Initio Calculations. *J. Am. Chem. Soc.* **1999**, *121*, 9343−9351.

(12) Atwood, C. G.; Geiger, W. E. Investigations of Time-Dependent Delocalization and the Correlation of Carbonyl IR Shifts with ΔE1/2 Values for Hydrocarbon-Linked Class II and Class III Mixed-Valent Complexes. *J. Am. Chem. Soc.* **2000**, *122*, 5477−5485.

(13) Stoll, M. E.; Geiger, W. E. In-Situ IR Spectroelectrochemistry Study of One-Electron Oxidations of Bis(Cyclopentadienyl) Molybdenum(II)−Alkyne or −Alkene Compounds. *Organometallics* **2004**, *23*, 5818−5823.

(14) Halet, J.-F.; Lapinte, C. Charge Delocalization vs Localization in Carbon-Rich Iron Mixed-Valence Complexes: A Subtle Interplay between the Carbon Spacer and the (Dppe)Cp*Fe Organometallic Electrophore. *Coord. Chem. Rev.* **2013**, *257*, 1584−1613.

(15) Low, P. J. Twists and Turns: Studies of the Complexes and Properties of Bimetallic Complexes Featuring Phenylene Ethynylene and Related Bridging Ligands. *Coord. Chem. Rev.* **2013**, *257*, 1507−1532.

(16) Tanaka, Y.; Akita, M. Organometallic Radicals of Iron and Ruthenium: Similarities and Dissimilarities of Radical Reactivity and Charge Delocalization. *Coord. Chem. Rev.* **2019**, *388*, 334−342.

(17) Tanaka, Y.; Ozawa, T.; Inagaki, A.; Akita, M. Redox-Active Polyiron Complexes with Tetra(Ethynylphenyl) Ethene and [2,2]-Paracyclophane Spacers Containing Ethynylphenyl Units: Extension to Higher Dimensional Molecular Wire. *Dalton Trans.* **2007**, *9*, 928−933.

(18) Mishiba, K.; Ono, M.; Tanaka, Y.; Akita, M. A Fully Charge-Delocalized Two-Dimensional Porphyrin System with Two Different Class III States. *Chem.—Eur. J.* **2017**, *23*, 2067−2076.

(19) Oyama, Y.; Kawano, R.; Tanaka, Y.; Akita, M. Dinuclear Ruthenium Acetylide Complexes with Diethynylated Anthrahydroquinone and Anthraquinone Frameworks: A Multi-Stimuli-Responsive Organometallic Switch. *Dalton Trans.* **2019**, *48*, 7432−7441.

(20) Fox, M. A.; Le Guennic, B.; Roberts, R. L.; Brue, D. A.; Yufit, D. S.; Howard, J. A. K.; Manca, G.; Halet, J.-F.; Hartl, F.; Low, P. J. Simultaneous Bridge-Localized and Mixed-Valence Character in Diruthenium Radical Cations Featuring Diethynylaromatic Bridging Ligands. *J. Am. Chem. Soc.* **2011**, *133*, 18433−18446.

(21) Parthey, M.; Gluyas, J. B. G.; Fox, M. A.; Low, P. J.; Kaupp, M. Mixed-Valence Ruthenium Complexes Rotating through a Conformational Robin−Day Continuum. *Chem.—Eur. J.* **2014**, *20*, 6895−6908.

(22) Fox, M. A.; Roberts, R. L.; Khairul, W. M.; Hartl, F.; Low, P. J. Spectroscopic Properties and Electronic Structures of 17-Electron Half-Sandwich Ruthenium Acetylide Complexes, [Ru(CCAr)(L2)-Cp′]+ (Ar=phenyl, p-Tolyl, 1-Naphthyl, 9-Anthryl; L2=(PPh3)2, Cp′=Cp; L2=dppe; Cp′=Cp*). *J. Organomet. Chem.* **2007**, *692*, 3277−3290.

(23) Fox, M. A.; Farmer, J. D.; Roberts, R. L.; Humphrey, M. G.; Low, P. J. Noninnocent Ligand Behavior in Diruthenium Complexes Containing a 1,3-Diethynylbenzene Bridge. *Organometallics* **2009**, *28*, 5266−5269.

(24) Alonso, A. G.; Reventós, L. B. Cyclopentadienylruthenium Complexes with Sulphur Donor Ligands: II. A Comparative Study of the Reactivity of Ru(η-RC5H4)Cl(L)2 (R = H, CH3, CH3CO; L = CO, Ph2PCH2CH2PPh2/2, P(CH2CH2CN)3) towards Anionic (S-S) Donor Ligands. *J. Organomet. Chem.* **1988**, *338*, 249−254.

(25) Bruce, M.; Wallis, R. Cyclopentadienyl-Ruthenium and-Osmium Chemistry. IX. Some Substituted H1-Vinylidene and H1-Acetylide Complexes. *Aust. J. Chem.* **1979**, *32*, 1471−1485.

(26) The DFT calculation of diethynylbenzene shows almost forbidden symmetric ν(C≡C) vibration (*f* = 0.0003). The DFT calculation was performed at the B3LYP/6-31G(d) level.

(27) Bruce, M. I.; Humphrey, M. G.; Snow, M. R.; Tiekink, E. R. T. Cyclopentadienyl-Ruthenium and -Osmium Chemistry: XXVII. X-Ray Structures of Ru(C≡CPh)(Dppe)(η-C5H5) and of [Ru(L)-(PPh3)2(η-C5H5)]X (L = C(OMe)Et, X = PF6; L = C≡CMePh, X = I). *J. Organomet. Chem.* **1990**, *397*, 187.

(28) Armitt, D. J.; Gaudio, M.; Skelton, B. W.; White, A. H.; Halet, J.-F.; Roberts, R. L.; Low, P. J.; Halet, J.-F.; Fox, A.; Roberts, L.; Hartl, F.; Low, J. Some Transition Metal Complexes Derived from Mono- and Di-Ethynyl Perfluorobenzenes. *Dalton Trans.* **2008**, 6763−6775.

(29) Gauthier, N.; Tchouar, N.; Justaud, F.; Argouarch, G.; Cifuentes, M. P.; Toupet, L.; Touchard, D.; Halet, J.-F.; Rigaut, S.; Humphrey, M. G.; Costuas, K.; Paul, F. Bonding and Electron Delocalization in Ruthenium(III) σ-Arylacetylide Radicals [Trans-Cl(H2-Dppe)2RuC≡C(4-C6H4X)]+ (X = NO2, C(O)H, C(O)Me, F, H, OMe, NMe2): Misleading Aspects of the ESR Anisotropy. *Organometallics* **2009**, *28*, 2253−2266.

(30) Parthey, M.; Kaupp, M. Quantum-Chemical Insights into Mixed-Valence Systems: Within and beyond the Robin−Day Scheme. *Chem. Soc. Rev.* **2014**, *43*, 5067−5088.

(31) Grevels, F.-W.; Kerpen, K.; Klotzbücher, W. E.; McClung, R. E. D.; Russell, G.; Viotte, M.; Schaffner, K. The Very Low Barrier of CO Site Exchange in Tricarbonyl(H4-1,5-Cyclooctadiene)Iron: Picosecond Kinetics in Solution Investigated by Line Shape Simulation of the ν(CO) IR Bands and Complementary Evidence from the Course of 13CO Incorporation in a Low-Temperature Matrix. *J. Am. Chem. Soc.* **1998**, *120*, 10423−10433.

(32) We made attempts to fit the spectrum with the assumption that the peak consists of two different peaks due to rotamers, and, however, the attempts were failed.

(33) The spectral changes upon the oxidation of m-1b are similar to those with *m*-**1a**.

(34) While a couple of rotamers afford the multiple NIR bands, those giving the major NIR bands can be classified into charge-delocalized species.

(35) For the estimation of V_{ab} of class II compounds, the donor-acceptor distance should be taken into account. Because, however, the charge is delocalized, the exact distance is hardly determined. For details see refs 36 and 37.

(36) Silverman, L. N.; Kanchanawong, P.; Treynor, T. P.; Boxer, S. G. Stark Spectroscopy of Mixed-Valence Systems. *Proc. R. Soc. London, Ser. A* **2008**, *366*, 33−45.

(37) Heckmann, A.; Lambert, C.; Goebel, M.; Wortmann, R. d. Synthesis and Photophysics of a Neutral Organic Mixed-Valence Compound. *Angew. Chem., Int. Ed.* **2004**, *43*, 5851−5856.

(38) ESR spectra of *p*-**1a,b**$^+$ observed as CH_2Cl_2 solutions at room temperature contained the broadened isotropic signals, which suggest the significant contribution of the organic ligand-based radical.

(39) Paul, F.; Ellis, B. G.; Bruce, M. I.; Toupet, L.; Roisnel, T.; Costuas, K.; Halet, J.-F.; Lapinte, C. Bonding and Substituent Effects in Electron-Rich Mononuclear Ruthenium σ-Arylacetylides of the Formula [(H2-Dppe)(H5-C5Me5)Ru(C:C)-1,4-(C6H4)X][PF6]n (n = 0, 1; X = NO2, CN, F, H, OMe, NH2). *Organometallics* **2006**, *25*, 649−665.

(40) Brunschwig, B. S.; Creutz, C.; Sutin, N. Optical Transitions of Symmetrical Mixed-Valence Systems in the Class II−III Transition Regime. *Chem. Soc. Rev.* **2002**, *31*, 168−184.

(41) Pangborn, A. B.; Giardello, M. A.; Grubbs, R. H.; Rosen, R. K.; Timmers, F. J. Safe and Convenient Procedure for Solvent Purification. *Organometallics* **1996**, *15*, 1518−1520.

(42) Hallman, P. S.; Stephenson, T. A.; Wilkinson, G. Tetrakis-(Triphenylphosphine)Dichlororuthenium(II) and Tris-(Triphenylphosphine)Dichlororuthenium(II). In *Inorganic Syntheses*; John Wiley & Sons, Ltd, 1970; pp 237−240.

(43) Frisch, M. J.; Trucks, G. W.; Schlegel, H. B.; Scuseria, G. E.; Robb, M. A.; Cheeseman, J. R.; Scalmani, G.; Barone, V.; Petersson, G. A.; Nakatsuji, H.; Li, X.; Caricato, M.; Marenich, A. V.; Bloino, J.; Janesko, B. G.; Gomperts, R.; Mennucci, B.; Hratchian, H. P.; Ortiz, J. V.; Izmaylov, A. F.; Sonnenberg, J. L.; Williams-Young, D.; Ding, F.; Lipparini, F.; Egidi, F.; Goings, J.; Peng, B.; Petrone, A.; Henderson, T.; Ranasinghe, D.; Zakrzewski, V. G.; Gao, J.; Rega, N.; Zheng, G.; Liang, W.; Hada, M.; Ehara, M.; Toyota, K.; Fukuda, R.; Hasegawa, J.; Ishida, M.; Nakajima, T.; Honda, Y.; Kitao, O.; Nakai, H.; Vreven, T.; Throssell, K.; Montgomery, J. A., Jr.; Peralta, J. E.; Ogliaro, F.; Bearpark, M. J.; Heyd, J. J.; Brothers, E. N.; Kudin, K. N.; Staroverov, V. N.; Keith, T. A.; Kobayashi, R.; Normand, J.; Raghavachari, K.; Rendell, A. P.; Burant, J. C.; Iyengar, S. S.; Tomasi, J.; Cossi, M.; Millam, J. M.; Klene, C.; Adamo, C.; Cammi, R.; Ochterski, J. W.; Martin, R. L.; Morokuma, K.; Farkas, O.; Foresman, J. B.; Fox, D. J. *Gaussian 16*, Revision B.01; Gaussian, Inc.: Wallingford CT, 2016.

(44) Renz, M.; Theilacker, K.; Lambert, C.; Kaupp, M. A Reliable Quantum-Chemical Protocol for the Characterization of Organic Mixed-Valence Compounds. *J. Am. Chem. Soc.* **2009**, *131*, 16292−16302.